

Contemporary ground deformation in the Taupo Rift and Okataina Volcanic Centre from 1998 to 2011, measured using GPS

L. Holden,¹ L. Wallace,² J. Beavan,^{3,†} N. Fournier,⁴ R. Cas,¹ L. Ailleres¹ and D. Silcock⁵

¹School of Earth, Atmosphere & Environment, Monash University, Melbourne, Victoria, Australia. E-mail: lucas.holden@monash.edu

²Institute for Geophysics, The University of Texas at Austin, Austin, TX, USA

³GNS Science, PO Box 30-368, Lower Hutt 5040, New Zealand

⁴GNS Science, Private Bag 2000, Taupo 3352, New Zealand

⁵School of Mathematical and Geospatial Science, RMIT University, Melbourne, Australia

Accepted 2015 June 5. Received 2015 May 18; in original form 2014 December 29

SUMMARY

The Taupo Volcanic Zone (TVZ) is one of the world's most productive regions of rhyolitic volcanism and contains the highly active Okataina Volcanic Centre (OVC). Within the TVZ, intra-arc extension is expressed as normal faulting within a zone known as the Taupo Rift. The OVC is located within a complex part of the rift, where volcanism and deformation is considered influenced by rift structure and kinematics. There has been significant research on the structural, volcanic and geophysical properties of the rift and OVC, but less focus on deformation using geodetic data. The limited studies that have utilized geodetic data do not clearly resolve the distribution of deformation and strain rates within the rift and OVC. This is essential to ensure that deformation signals from volcanic processes at the OVC are correctly identified and distinguished from those related to regional tectonic or local hydrothermal processes within the rift. In this paper, we present a picture of contemporary deformation at the OVC and within the surrounding rift in detail, using existing and new GPS campaign and continuous GPS (cGPS) data collected between 1998 and 2011. The results show a highly heterogeneous deformation and strain rate field (both extension and shortening) through the study area, partitioned into different parts of the rift. Our results agree well with earlier geodetic studies, as well as identify new features, but some deformation patterns conflict with long-term geological observations. In the OVC, we observe a locally rotated horizontal velocity field, significant vertical deformation and variable strain rates across the caldera. In the Tarawera Rift, we identify elevated extension and shear rates, which may have significant implications for volcanism there. A shortening pattern is identified through the central rift, which is unexpected in an intra-arc rifting environment. We attempt to explain the source/s of shortening and extension and discuss their implications for geodetic monitoring efforts in the OVC.

Key words: Satellite geodesy; Volcanic arc processes.

INTRODUCTION

Within large caldera systems, geodetic observations can provide accurate measurements of ground deformation. These observations can be studied to better understand magma system dynamics and related volcanic processes. However, they must be interpreted within the regional context, as tectonic, magmatic or hydrothermal activity can mask volcanic deformation signals. In magmatically active rift

systems this is challenging, as studies have implied the presence of complex inter-relationships between magmatism, tectonics and volcanism, whereby magmatism and upper crustal deformation can feedback on one another (Manville & Wilson 2003; Spinks *et al.* 2005; Wilson & Charlier 2009; Acocella 2010; Kogan *et al.* 2012; Keir *et al.* 2013). To interpret local deformation at large caldera systems in active rift settings, accurate models of the regional velocity and strain rate field are necessary.

The Okataina Volcanic Centre (OVC) is a large inter-rift caldera, located in a complex tectonic rift setting known as the Taupo Volcanic Zone (TVZ). This is a region of active tectonic extension

† Deceased.

(Darby *et al.* 2000; Wallace *et al.* 2004), high heat flow and magmatism (Bibby *et al.* 1995) and is one of the most productive regions of rhyolitic volcanism in the world (Wilson *et al.* 1995; Sutton *et al.* 2000; Price *et al.* 2005). The OVC is one of seven large caldera centres in the TVZ that have produced very large eruptions and it is the most recently active volcanic region of the TVZ (Houghton *et al.* 1995; Wilson *et al.* 1995). Geodetic monitoring at the OVC is currently undertaken using cGPS stations permanently within and around the caldera. These are complemented with repeated campaign style GPS surveys. This monitoring must be accompanied by an understanding of what is likely to happen during renewed activity, as well as the ability to discriminate between such activity and background rifting processes (Ellis *et al.* 2007).

The last eruption within the OVC (the 1886 Tarawera eruption) was preceded by only one hour of felt earthquakes (Nairn 2002). Although seismicity is monitored at the OVC with a network of seismographs, increased seismic noise may be interpreted as normal tectonic activity, which characterizes this region (Bryan *et al.* 1999). As a result, seismic monitoring cannot be solely relied upon and should be used alongside other techniques such as geodetic monitoring. However, geodetic data indicating ground deformation must be interpreted with caution. Since there has been no recent significant activity at the OVC, the geodetic precursors leading to a volcanic crisis remain relatively unknown. Also, the use of precise GPS monitoring of volcanic systems implies that the observations will record both a local signal (assumed to be due to magmatic and/or hydrothermal processes) and a regional tectonic signal (Cabral-Cano *et al.* 2008). Further, a number of highly active geothermal fields exist within and around the OVC, whose recurrent activity must be considered when interpreting deformation.

In the TVZ, intra-arc extension is accommodated pre-dominantly by a zone of normal faulting, dyke intrusion and extensional fracturing, known as the Taupo Rift (Acocella *et al.* 2003; Villamor & Berryman 2006). Studies suggest that the rift is divided into discrete segments with variable extension rates and styles as well as different upper crustal properties (Rowland & Sibson 2001; Acocella *et al.* 2003; Rowland *et al.* 2010). The Okataina segment occurs at the largest stepover in the Taupo Rift (see Fig. 1) and is considered to be either a structurally complex transfer zone related to local strain adjustment (Acocella *et al.* 2003; Cole & Spinks 2009; Cole *et al.* 2010) or an accommodation zone that reflects stress field heterogeneity (Rowland & Sibson 2001; Rowland *et al.* 2010).

It is not clear how regional tectonic structure, rift kinematics and magmatic processes relate to deformation patterns and volcanism at the OVC. Wilson & Charlier (2009) propose that in this region of the rift, complex interactions between magmatism and tectonic processes exist, whereby magma emplacement mediates crustal deformation, while rift related normal faulting can control magma emplacement. Seebek & Nicol (2009) propose that crustal extension is tectonic outside the OVC and induced by dyke intrusion within the caldera boundary. Rift structure and kinematics have been linked to OVC caldera structure and development, eruptive behaviour and volcanism (Cole *et al.* 2005, 2010; Smith *et al.* 2005, 2010; Cole & Spinks 2009). Rowland & Sibson (2001) question whether the magma localization at the OVC is a result of stress heterogeneity in the Okataina segment (linked to a step in rift structure) or if there is another cause still remains uncertain.

Studies using geodetic data within New Zealand's North Island and Taupo Rift have been limited, but have provided a better understanding of the regional velocity field (Beavan & Haines 2001) and rifting rates (Darby *et al.* 2000; Wallace *et al.* 2004). Recently, Differential Radar Interferometry (InSar) data have been utilized to

examine the broad scale patterns between surface uplift and subsidence and magmatism at a large scale across the central North Island (Samsonov *et al.* 2011; Hamling *et al.* 2015). However, these studies do not provide a detailed picture of the horizontal and vertical velocity and strain rate fields through the entire central Taupo Rift. As a result, there is limited knowledge about deformation patterns through the Taupo Rift and it remains difficult to identify ground deformation patterns within the OVC linked to volcanic processes there.

In this paper we reprocess 11 yr of continuous and campaign GPS data (including new data) for the central and northern Taupo Rift and OVC. Incorporating this new data, we present a new picture of contemporary crustal deformation through this region and across the OVC. This includes the first published strain field for the TVZ from a comprehensive GPS velocity field. We consider and discuss the various origins of the deformation patterns and their implication for monitoring volcanic processes at the OVC. Specifically, we address the following specific questions; (1) what is the nature of contemporary ground deformation through the OVC and in the surrounding Taupo Rift and (2) is deformation in the OVC related to volcanic activity or linked to background tectonic processes or local hydrothermal activity? Finally, we discuss the implications of our results for geodetic monitoring of volcanic activity in the OVC.

RIFT STRUCTURE AND KINEMATICS

Intra-arc rifting processes in the Taupo Rift have been linked to rapid tectonic block rotation along the eastern North Island (Wallace *et al.* 2004). This region is characterized by a strain rate field that is primarily extensional (Beavan & Haines 2001). Geodetic (GPS) observations have measured varying total rates of extension along the rift axis, from $\sim 15 \text{ mm yr}^{-1}$ near the Bay of Plenty to $\sim 7 \text{ mm yr}^{-1}$ in the Lake Taupo area (see Fig. 1; Wallace *et al.* 2004). Wallace *et al.* (2004) interpret these results to indicate a uniformly decreasing (southwards) wedge based extension model though the central North Island. Rowland *et al.* (2010) correctly point out that these results reflect bulk movement of the eastern North Island away from the fixed Australian Plate and that the distribution of contemporary strain within the TVZ is not well resolved in the previously published geodetic studies. Alternatively, Villamor & Berryman (2001, 2006) propose a more parallel-sided extension model with abrupt changes at specific locations along the rift axis, although with an overall northward increase in extension rates. Mouslopoulou *et al.* (2007) propose that the increase in extension rate near the Bay of Plenty (see Fig. 1) is a result of the interaction and transfer of strike-slip fault motion from the North Island Dextral Fault Belt (NIDFB) (see Fig. 1) into the rift structure.

The modern Taupo Rift is divided into a number of offset and variably oriented rift segments that are either soft linked by accommodation zones of stress heterogeneity (Rowland & Sibson 2001) or hard linked by transfer faults (Acocella *et al.* 2003). Following Acocella *et al.* (2003), these include the Whakatane, Okataina, Kapenga, Taupo and Ruapehu segments (see Fig. 1). The axial part of the rift is roughly symmetrical with a central graben axis (Cole & Spinks 2009) and contains a dense array of normal faults between the Okataina and Taupo Volcanic Centres, known as the Taupo Fault Belt (TFB; Grindley 1960; see Fig. 1). Shallow upper crustal seismicity is primarily concentrated within this area (Bibby *et al.* 1995; Ellis *et al.* 2007). In the central TVZ, Rowland *et al.* (2010) propose that extensional mechanisms vary and include: pure tectonic faulting, mafic and rhyolitic dyke intrusion, regional scale uplift

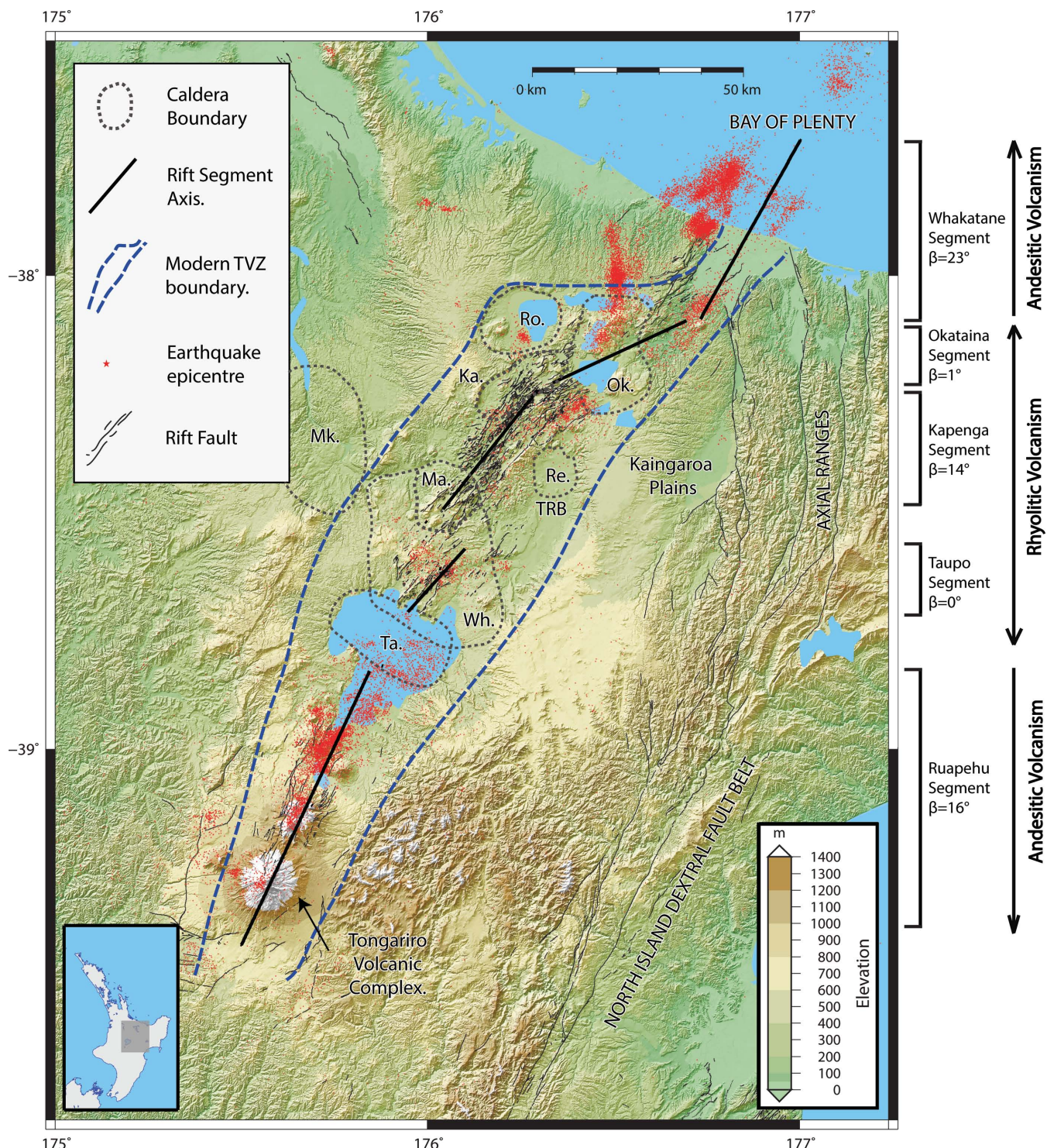


Figure 1. Structural diagram of the Taupo Rift. The modern TVZ boundaries are approximate and from Cole (1990). Rift segment axis and dextral shear diagrams from Acocella *et al.* (2003). Light black lines are active rift faults from the GNS Science Active Faults Database. Epicentres plotted for shallow earthquakes (<10 km) between 1998 and 2011 from the GNS Science GeoNet Earthquake Database. DEM produced using LRIS Data Portal from NZ Landcare Research. Caldera boundary locations are shown as dashed grey lines and are approximate. Ro. Rotorua Caldera, Ok. Okataina Caldera, Mk. Mangakino Caldera, Ma. Maroa Caldera, Re. Reporoa Caldera, Ta. Taupo Caldera, To. Tongariro Volcanic Complex, Wh. Whakamaru Caldera. Dashed blue lines represent modern rift boundaries (from Acocella *et al.* 2003). Bottom left inset shows location of study area.

and transient subsidence associated with inflation or deflation of mafic magma bodies and regional-scale basin development in association with rhyolitic caldera-forming eruptions. They divide this region into two parallel zones (see Fig. 1): a cooler western belt that

deforms by faulting (i.e. the TFB) and a warmer zone (the Taupo Reporoa Basin—TRB) of little surface faulting, high heat flow and possibly partial melt in the upper crust. East of the Taupo Rift lies the Axial Ranges (see Fig. 1), where strike-slip faulting dominates

(e.g. Beanland & Haines 1998) and largely coincides with the Axial Ranges (AXIR) tectonic block of Wallace *et al.* (2004).

Geological studies indicate different components of dextral shear and extension along the rift (see Fig. 1; Acocella *et al.* 2003). Studies also show that segments with high extension rates (the Okataina and Taupo segments) correspond to the highly active rhyolitic Taupo and Okataina volcanic complexes, while segments with a high degree of trans-tensional shear (Whakatane, Kapenga and Ruapehu segments) coincide with more moderately eruptive andesitic stratovolcanoes (Acocella *et al.* 2003; Spinks *et al.* 2005). The Okataina segment connects the neighboring parallel Whakatane and Kapenga (Ngakuru) grabens by obliquely trending fault and vent lineations, which is accommodated by curved faults and is also characterized by a slight trend (~ 20 deg) variation in the extension direction (orthogonal to Okataina structures with respect to neighboring segments) (Acocella *et al.* 2003). This segment occurs at the largest step in the Taupo Rift (Rowland & Sibson 2001; Acocella *et al.* 2003; Cole & Spinks 2009; Cole *et al.* 2010). Rowland & Sibson (2001) consider these structural variations a result of stress heterogeneity linked to accommodation zones and question whether this is the cause of magmatic localization at the OVC or an effect of magmatism. Acocella *et al.* (2003) suggest that the more easterly change in segment orientation is not sufficient to account for all the trend rotation and propose the presence of a local rotation due to local readjustment of strain between the interacting Whakatane and Kapenga offset segments.

A broad wavelength (~ 250 km), dome shaped pattern of rock uplift, centred east of Mt Ruapehu in the Tongariro Volcanic Complex (see Fig. 1), dominates the vertical tectonics of the central North Island (Pulford & Stern 2004). They link this uplift to thermal processes in the underlying mantle wedge. In contrast, within the central rift, subsidence patterns are observed to vary in space and time and have been linked to rifting processes and magma availability (Villamor & Berryman 2001; Manville & Wilson 2003; Rowland *et al.* 2010; Hamling *et al.* 2015). Subsidence in the Whakatane segment, associated with rifting, has been measured at $1\text{--}2\text{ mm yr}^{-1}$ at the Bay of Plenty coast and uplift of $0.5\text{--}1\text{ mm yr}^{-1}$ at the eastern and western margins of the rift in this region (Wright 1990). In the Kapenga segment, subsidence rates have locally been estimated at $-7.23 \pm 0.38\text{ mm yr}^{-1}$ from fault displacement (Villamor & Berryman 2001) and up to -10 mm yr^{-1} from repeated precise levelling (Blick & Otway 1995). Immediately north of Taupo caldera, local vertical deformation is small (relative to the Taupo Rift further northwards), appears to be episodic on a scale between 1 and 10 yr, and is often associated with magma migration (Manville & Wilson 2003). InSar has also identified localized regions of subsidence linked to geothermal exploitation (Hole *et al.* 2005, 2007; Samsonov *et al.* 2011).

THE OKATAINA VOLCANIC CENTRE

The OVC is a rectangular caldera structure whose long axis trends roughly perpendicular to the Okataina segment axis (see Fig. 2) (Spinks *et al.* 2005). It consists of overlapping and nested caldera structures filled with post-caldera rhyolites, which includes the larger Haroharo caldera (delineated by the bold line in Fig. 2), containing the Haroharo and Tarawera volcanic complexes (Nairn 2002). Eruptive vents post 25 ka are well mapped and define two broad linear zones; the Tarawera and Haroharo linear vent zones (see Fig. 2; Nairn 2002). These lineations are roughly axial to the Whakatane and Kapenga segments and considered to mark their

continuation into the Okataina area (Spinks *et al.* 2005). Volcanic activity within the last 26 ka has been linked to post-caldera rhyolitic dome building (Cole *et al.* 2010), primarily along these linear vent zones (Nairn 2002). Recent volcanic activity includes the 1886 AD Tarawera–Rotomahana–Waimangu basalt dyke intrusion eruption from the Tarawera volcanic complex. Today the most intense hydrothermal activity is located outside the caldera, within the Lake Rotomahana, Waimangu and the Waiotapu geothermal fields (see Fig. 2), and it is closely related with the southwest extension of the Tarawera vent lineations and 1886 AD rift (Nairn 2002). A number of small to moderate hydrothermal explosions have occurred within these fields since 1886 (Scott 1992, 1994; Vandemeulebrouck *et al.* 2008).

The 1886 AD eruption was preceded by only one hour of felt earthquakes and no eyewitness reports exist of pre-eruptive ground deformation patterns (Nairn & Cole 1981). Sherburn & Nairn (2004) hypothesize two types of ground deformation might precede a surface dyke intrusion at the OVC similar to the 1886 event: the first reflecting the rapidly increasing loss of magma at depth, and the second reflecting dyke intrusion much closer to the surface. They believe this signal would consist of a longer wavelength, deep deflation signal, superimposed by shallow shorter wavelength inflation. They suggest that monitoring sites on the upper slopes of Mt. Tarawera would probably record uplift (due to the dyke intrusion); however more distant sites would only detect the effect of the deeper deflation source, and measure subsidence. They further note that a small (1 per cent) volumetric inflation of the rhyolitic magma chamber would be detected by the lake levelling network, however if this inflation occurred at a steady rate over several years, it would initially be interpreted as tectonic in origin.

Geodetic observations, including lake and tilt levelling measurements plus horizontal strain rate network measurements have measured ground deformation within the caldera (Scott 1989). Scott (1989) measured significant shear strain rate ($1.66 \pm 1.6\text{ ppm yr}^{-1}$) and dilation ($-4.33 \pm 0.9\text{ ppm yr}^{-1}$) near Lake Rotomahana (see Fig. 2), (where negative dilational strain rate is linked to contraction). Scott (1989) emphasized that these results may have been biased by short observation intervals, but still concluded that significant deformation was occurring within the Tarawera Rift. cGPS sites are operated by GeoNet (www.geonet.org.nz) within the caldera. At present, there are seven cGPS receivers stationed within and around the OVC (see Fig. 3). However it should be noted that some of these instruments have only been in operation since 2009. Recent studies using InSAR (Samsonov *et al.* 2011; Hamling *et al.* 2015) has detected broad subsidence across the OVC region, which these studies interpret to be of volcanic or magmatic origin.

GPS DATA

GNS Science has surveyed a large geodetic network in the central North Island since the early 1990s (Darby & Williams 1991; Darby & Meertens 1995). Various sections of this network have been measured every 1–4 yr by GPS campaign surveys. The majority of geodetic stations in this network consist of concrete blocks with brass plaques anchored in bedrock. In addition, an extensive network of cGPS sites has also been installed and operated across NZ by GeoNet (www.geonet.org.nz) and Land Information New Zealand (LINZ), for both geodetic/surveying and geophysical monitoring applications. We analyse data collected from eight GPS campaign surveys (57 geodetic stations) conducted between 1998 and 2011 and data from the two continuous networks (21 stations in total) of

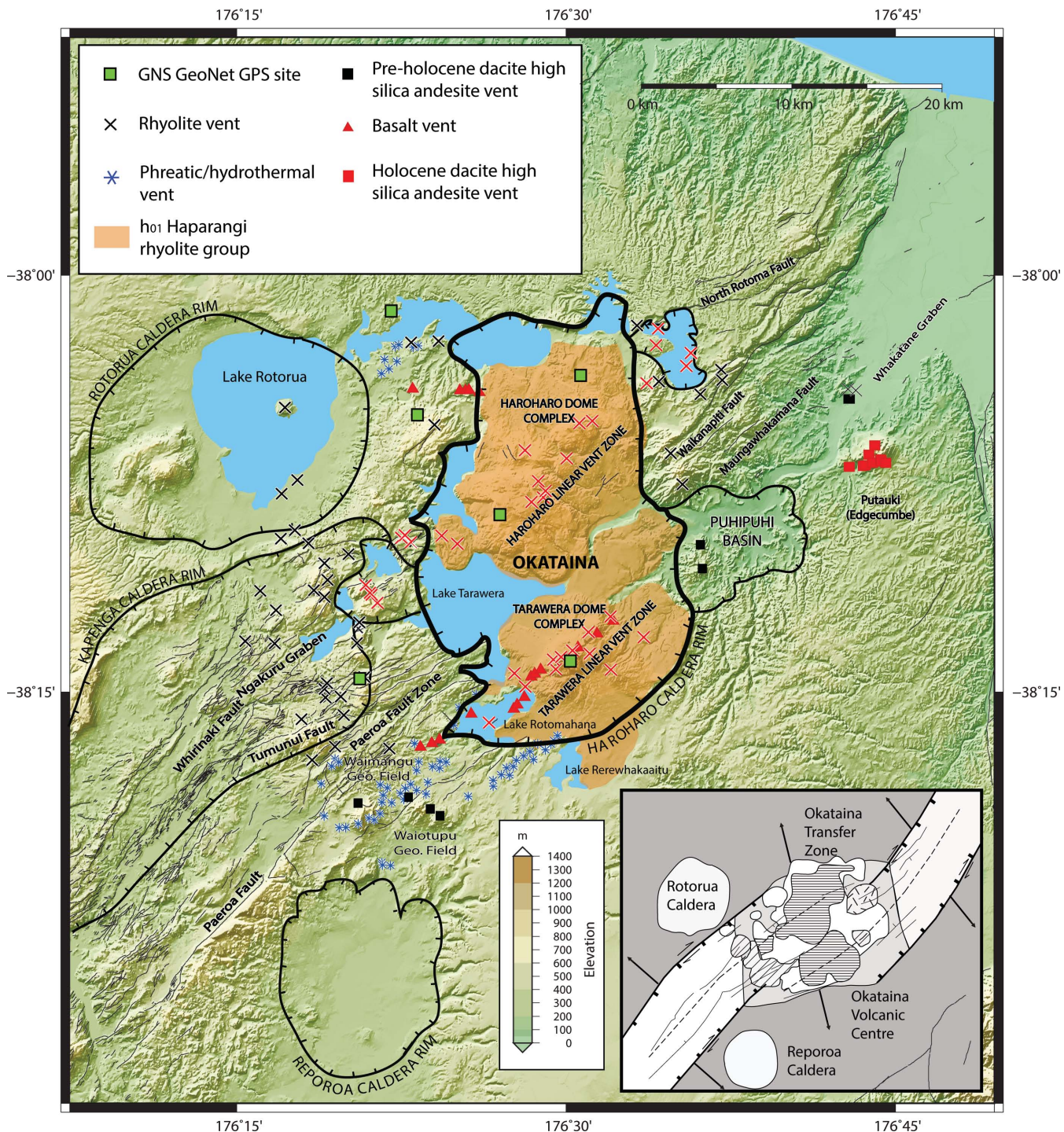


Figure 2. Location map and structural details of the Okataina Volcanic Centre (OVC) from Nairn (2002). Caldera boundary locations are shown as dashed grey lines and from Spinks *et al.* (2005). Bottom right inset shows interaction of the Okataina Rift segment and OVC with the neighboring Kapenga and Whakatane Rift segments (from Cole *et al.* 2010).

the same time period. The location of all these stations is illustrated in Fig. 3. The occupation details of the geodetic stations occupied in these campaigns are shown in Table 1. For campaign surveys from 2000 to 2011, stations were occupied for two days consecutively (20–24 hr each day). For earlier campaigns, before 2000, some sessions are 7–8 hr in length. Trimble GPS receivers (Trimble 4000 series, 5700 and R7s) and Trimble antennas (mostly Zephyr Geodetic, but some Choke rings for the earlier measurements) have

been used predominantly for all campaign surveys and continuous sites, with some Ashtech receivers used in the earlier campaigns.

We also include regional cGPS data from International Geodynamics Service (IGS) sites in New Zealand, Australia and the southwest Pacific in our processing in order to obtain GPS velocities as a consistent solution in a well-defined reference frame (see Fig. 3). GPS processing was performed using IGS *Reproj* products (precise orbits, clock corrections and Earth rotation

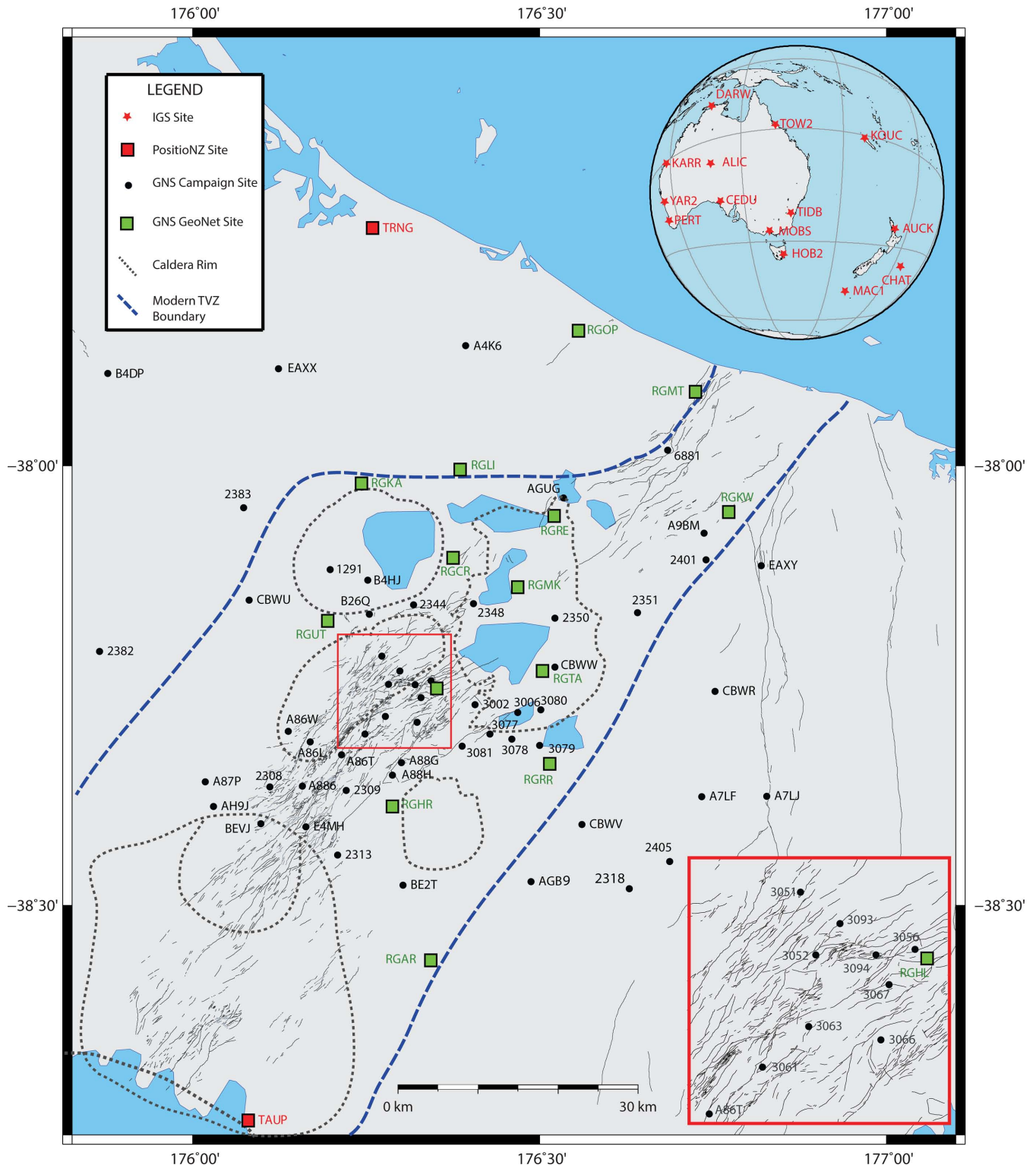


Figure 3. Location and distribution of all GPS stations used in this processing. Locations of calderas are shown as dashed grey lines and are approximate. Modern TVZ boundaries are approximate. IGS GPS stations are plotted on globe at top right. Bottom right inset shows GPS stations southwest of OVC in greater detail.

parameters). These products are the result of the re-analysis of all GPS data collected by the IGS network since 1994 using a consistent approach (International GNSS Service 2012). The benefit of these products is that they are all aligned with one reference frame and account for absolute antenna calibrations. The

final station coordinates and velocities for this study are in the IGS08 reference frame. We then transform these results to a local fixed reference frame to better identify the ground deformation within the study area (this is described in more detail in the next section).

Table 1. History of occupation for campaign sites processed. SITE: four character code description of campaign site. X: each X represents one daily occupation each year with the exception of some 1998/1999 campaigns. XXXXX* indicates that more than five occupations were observed in the calendar year of the campaign. This is the case when two or more campaigns are conducted at different times in the calendar year.

Site	Occupation details							
	1998	1999	2000	2001	2005	2007	2009	2011
1291			XX		XX	XX		XX
2308		XXX		XX	XX		XX	
2309		XX		XX	XX			XX
2313		XXX		XX	XXXX			XX
2318		XX		XX	XX			XX
2344		XX		XXX	XX			XX
2348		XX		XX	XX			XX
2350		X		XX	XX			XX
2351		X		XX	XX			XX
2382				XXX	XX			XX
2383		XX		XX	XX			XX
2401			X	X	XXXX			
2405		XX		X				
3002		XX		XXX	XX			XX
3006		XX		XX	XX			XX
3051	XXX	XXXXX*	XXXXX*	XXXXX*	XX	XX		XX
3052		XX		XX	XX			XX
3056		XX		XX	XX			XX
3061		XX		XX	XX			XX
3063		XX		XX	XX			XX
3066		XX		XX	XX			XX
3067		XX		XX	XX			XX
3077		XX		XX	XX			XX
3078		XXX		XX	XX			XX
3079		XX		XX	XX			XX
3080	XX	XXXXX*	XXXXX*	XXXXX*	XX	XX		XX
3081		XX		XX	XX			XX
3093		XX		XX	XX			XX
3094		XX		XX	XX			XX
6881					XX		XX	XX
A4K6					XX		XX	XX
A7LF		XX		XX	XX			XX
A7LJ		XX		XX	XX			XX
A86L		XX		XX	XX			XX
A86T					XXX	XX		XX
A86W					XX	XX		XX
A87P					XX	XX		XX
A88G		XX		XX	XX			XX
A88H		XX		XX	XX			XX
A886					XXX	XX		XX
A89V		XX		XX				
AGB9					XX	XX		XX
A9BM			XX		XX	XX		XX
AGUG					X	XX		XX
AH9J					XX		XX	XX
B26Q		XX			XX	XX		XX
B4DP					XX	XX		XX
B4HJ					X	XX		XX
BE2T		XX				XX	XX	XX
BEVJ	XX	XXXXX*	XXXXX*	XXXXX*	XX	XX		XX
CBWR		XX			XX	XX		XX
CBWU		XXX			XXX	XX		XX
CBVV		XX	XX		XXX	XX		XX
CBWW		XX			XX	XX	XX	
EAXX						XX	XX	XX
EAXY						XX	XX	XX
E4MH						XXX	XX	XX

GPS PROCESSING AND VELOCITY ESTIMATION

We use standard high precision processing procedures for the GPS phase processing in Bernese GPS software (BSW) version 5.0 (Dach *et al.* 2007). In the first part of the processing we obtain daily coordinate estimates and their associated covariance matrices using the double difference baseline processing strategy. We use IGS antenna phase centre models to account for different antenna types. Phase ambiguities are fixed using the quasi-ionospheric free resolution strategy. We use an elevation cut-off angle of 3 deg and elevation-dependent weighting in the observation modelling and parameter estimation. The DRY_NIELL model (Neil 1996) was used to estimate tropospheric parameters at 4-hr intervals. Normal equations were generated without fixing stations to their *a-priori* coordinates.

The normal equations are then combined (using the ADDNEQ2 option in BSW) in order to calculate station velocities. In ADDNEQ2, we first minimally constrain regional (Australia and NZ) IGS stations to their ITRF coordinates and velocities to identify any inconsistencies and check repeatability in these reference stations. Following this, we estimate final station velocities for our NZ campaign and continuous stations by tightly constraining the velocities of the IGS stations in ADDNEQ2. The results indicated that stations west and northwest of the Taupo Rift (e.g. stations 2381, 2383, B4DP and EAXX which are shown west and northwest of Rotorua caldera in Fig. 3) move with similar horizontal velocities (to within 1.1 mm yr⁻¹). We use these sites to define a local reference frame for the TVZ velocity field. We then determine GPS velocities through the study area relative to this local reference frame, through a transformation, minimizing their velocities to zero.

A recent study (Tregoning *et al.* 2013) shows some small motion of cGPS stations along the west coast of the North Island, relative to the fixed Australian Plate. Given the possibility that the western North Island has some motion relative to the Australian Plate (e.g. Tregoning *et al.* 2013) we prefer to view the velocity field relative to the stable crustal block just to the west of the TVZ, rather than relative to a fixed Australian Plate, as this gives us clearer insight into the kinematics within the central North Island. The sites we choose for our local reference frame are well suited for this, as they are observed for the full study period and the variations we observe between these stations are very small relative to the large displacements in the rift. In this study, we choose not to use GeoNet cGPS sites west of our study area to define our reference frame since many were not available at the start of our campaign data. Moreover, the determination of strain rates from GPS velocities is independent of reference frame (Sagiya *et al.* 2000) and we find our velocities to be in excellent agreement with the results presented in Beavan & Haines (2001) and Wallace *et al.* (2004) and cGPS sites maintained by GeoNet.

It is well documented that GPS formal velocity errors resulting from Bernese ADDNEQ2 are underestimated and at present there is no standard approach for appropriately rescaling these values (Hugentobler *et al.* 2001; Geirsson 2003; Kashani *et al.* 2004). Further, Bernese (BSW) 5.0 is unable to rescale the covariance matrices in the ADDNEQ2 process (Dach *et al.* 2007). Subsequently, our rescaling of the GPS formal velocity errors was performed externally of BSW. The use of BSW variance–covariance matrices for estimation of GPS velocity uncertainties results in underestimation, since no consideration is given to time-dependent errors such as random walk error and time-independent error such as white noise. The magnitude of these errors can be assessed using spectral analysis or maximum likelihood estimation (MLE) of suitably long contin-

uous GPS time series (see e.g. Zhang *et al.* 1997; Mao *et al.* 1999; Dixon *et al.* 2000; Williams *et al.* 2004; Beavan 2005). According to Zhang *et al.* (1997), velocity uncertainty related to random walk noise ($\sigma_{\hat{v}}$)_{WN} (mm yr⁻¹) is proportional to the magnitude of white noise (a_{WN}) in millimetres, and inversely proportional to the total observation internal T (years) and the square root of the number of measurements N , as shown in eq. (1) below;

$$(\sigma_{\hat{v}})_{WN} = \frac{2\sqrt{3}a_{WN}}{N^{1/2}T} \quad (1)$$

Zhang *et al.* (1997) estimate the component of velocity uncertainty related to random walk error ($\sigma_{\hat{v}}$)_{RWN} using eq. (2);

$$(\sigma_{\hat{v}})_{RWN} = \frac{b_{RWN}}{T^{1/2}} \quad (2)$$

whereby, ($\sigma_{\hat{v}}$)_{RWN} in mm yr⁻¹ is proportional to the magnitude of random walk noise amplitude b_{RWN} in mm yr^{-1/2} and inversely proportional to the square root of the total time span T . a_{WN} and b_{RWN} are obtained empirically from the MLE or spectral analysis techniques aforementioned.

In this study we are unable to empirically derive a_{WN} and b_2 from our campaign GPS data since our sampling number and sampling interval are poor (e.g. we do not have a suitably long continuous GNSS time series over the span of our study to estimate reliable results). As a result, our velocity uncertainties incorporate the estimates of Beavan (2005), who analysed the long-term noise characteristics of geodetic monuments in our study area. These are typical of, and in some cases are the same geodetic monuments we use in our study. Beavan (2005) derives mean white noise values (a_{WN}) of 1.1, 1.1 and 3.7 mm yr⁻¹ in the east, north and up components respectively. He also derives median random walk noise amplitudes (b_2) of 1.8, 2.1 and 4.1 mm yr^{-1/2} in the east, north and up components. We incorporate these values into our uncertainty estimates in Table 2.

Our horizontal and vertical velocities are illustrated in Figs 4 and 5. These results are also presented in detail in Table 2 along with their uncertainties. The horizontal velocities are in good agreement with those presented in Beavan & Haines (2001), Wallace *et al.* (2004), Beavan & Litchfield (2012), and Tenzer *et al.* (2012). We observe a small uniform rotation from their solutions due to selection of difference reference frames, as most of the previous velocity fields were shown in an Australian Plate fixed reference frame. We interpret our vertical velocities with caution, due to their inherently larger uncertainties, particularly from campaign style GPS data. In some instances our estimates are larger than prior estimates from geological measurements. However, we find an excellent agreement with the vertical velocities from differential levelling (Darby *et al.* 2000) and cGPS sites maintained by GeoNet (www.geonet.org.nz) and those presented in Samsonov *et al.* (2011) and Hamling *et al.* (2015), which indicates consistency in our approach.

RESULTS

Horizontal and vertical deformation

Figs 4–6 illustrate our horizontal and vertical deformation results. Sites east and southeast of the Taupo Rift, towards the AXIR tectonic block, move coherently southwards up to 15 mm yr⁻¹ with negligible vertical movement. In the Whakatane segment, velocities coherently trend southerly (e.g. stations RGMT and 6881), at rates between 7 and 9 mm yr⁻¹, which increase towards the AXIR tectonic block (e.g. stations RGKW and EAXY in Fig. 3). Sparse

Table 2. GPS velocities of TVZ sites (in millimetre per year, in the local fixed reference frame.) Site: four digit site code, Long.: Longitude of station ($^{\circ}$), Lat.: Latitude of station ($^{\circ}$), $V_E/V_N/V_{UP}$: east, north and up velocity respectively, $\sigma_{VE}/\sigma_{VN}/\sigma_{VUP}$ are the 1σ uncertainty of the respective velocities.

Site	Long.	Lat.	V_E	V_N	V_{UP}	σ_{VE}	σ_{VN}	σ_{VUP}	$ V_{hor} $	$\sigma V_{hor} $
HAMT	175.1092	-37.8068	-0.4	1.6	0.4	0.8	0.9	1.7	1.6	0.9
KTIA	173.2731	-35.0689	4.4	3.9	-0.8	1.2	1.3	2.7	5.9	1.2
MAHO	174.8541	-38.5130	-0.7	2.9	-2.4	0.8	0.9	1.7	3.0	0.9
RGAR	176.3430	-38.5620	-0.9	-4.0	-3.6	1.4	1.5	3.2	4.1	1.5
RGCR	176.3780	-38.1047	0.5	-3.8	-3.2	1.2	1.3	2.7	3.8	1.3
RGHL	176.3523	-38.2519	-4.3	-4.3	-19.6	1.4	1.5	3.2	6.1	1.4
RGHR	176.2880	-38.3858	-2.2	-4.6	-7.5	1.2	1.3	2.7	5.1	1.3
RGKA	176.2441	-38.0201	0.4	-1.6	-0.9	1.2	1.3	2.7	1.6	1.3
RGKW	176.7728	-38.0525	0.0	-10.4	-0.8	1.4	1.5	3.2	10.4	1.5
RGLI	176.3857	-38.0033	0.6	-3.4	-2.1	1.2	1.3	2.7	3.5	1.3
RGMK	176.4671	-38.1383	0.6	-9.0	-17.9	0.8	0.9	1.7	9.0	0.9
RGMT	176.7247	-37.9154	0.2	-8.2	10.4	1.4	1.5	3.2	8.2	1.5
RGOP	176.5563	-37.8459	-3.4	-2.0	4.5	1.2	1.3	2.7	3.9	1.2
RGRE	176.5212	-38.0573	-1.4	-5.3	-2.1	1.2	1.3	2.7	5.5	1.3
RGRR	176.5146	-38.3389	-1.4	-5.8	-1.9	1.2	1.3	2.7	6.0	1.3
RGTA	176.5061	-38.2338	-3.7	-2.6	-13.8	1.2	1.3	2.7	4.5	1.2
RGUT	176.1942	-38.1766	3.7	-3.4	-6.0	0.8	0.9	1.7	5.0	0.8
TAUP	176.0810	-38.7427	3.6	-4.5	1.6	0.8	0.9	1.7	5.8	0.8
TRNG	176.2609	-37.7288	1.1	-0.1	-0.9	0.8	0.9	1.7	1.1	0.8
WHNG	174.3146	-35.8038	2.4	2.3	0.3	0.8	0.9	1.7	3.3	0.8
1291	176.1979	-38.1184	1.6	-1.2	-5.5	0.5	0.6	1.2	2.0	0.6
2308	176.1110	-38.3652	4.1	-5.0	-9.1	0.8	0.9	1.9	6.5	0.8
2309	176.2211	-38.3693	-1.1	-4.3	-11.9	0.5	0.6	1.2	4.4	0.6
2313	176.2086	-38.4424	-3.1	-3.3	-19.4	0.7	0.7	1.6	4.5	0.7
2318	176.6344	-38.4847	1.0	-8.6	-2.1	0.5	0.6	1.2	8.7	0.6
2344	176.3181	-38.1582	-0.3	-4.8	-5.7	0.6	0.7	1.3	4.8	0.7
2348	176.4048	-38.1570	2.1	-3.5	-3.8	0.5	0.6	1.2	4.1	0.6
2350	176.5221	-38.1736	1.1	-5.6	-9.7	0.5	0.6	1.1	5.7	0.6
2351	176.6411	-38.1673	1.2	-6.6	-5.7	0.5	0.6	1.1	6.7	0.6
2382	175.8654	-38.2111	-0.6	-0.2	0.5	1.1	1.3	3.3	0.6	1.2
2383	176.0731	-38.0478	-0.1	-0.2	0.4	0.5	0.6	1.2	0.2	0.6
2401	176.7401	-38.1069	5.6	-4.2	-6.9	1.0	1.1	2.7	7.0	1.1
2405	176.7027	-38.4544	1.5	-9.4	2.5	0.8	0.9	1.9	9.5	0.9
3002	176.4069	-38.2719	2.0	-2.1	-19.4	0.6	0.7	1.3	2.9	0.6
3006	176.4683	-38.2807	-2.2	-3.9	-2.2	0.5	0.6	1.2	4.5	0.6
3051	176.2725	-38.2166	2.1	-4.7	-11.0	1.0	1.2	4.3	5.1	1.1
3052	176.2822	-38.2486	1.8	-3.4	-13.5	0.5	0.6	1.2	3.8	0.6
3056	176.3459	-38.2463	-1.2	-4.7	-14.0	0.5	0.6	1.2	4.9	0.6
3061	176.2483	-38.3054	0.6	-1.7	-12.9	0.5	0.6	1.2	1.8	0.6
3063	176.2779	-38.2850	1.2	-0.7	-12.2	0.5	0.6	1.2	1.4	0.6
3066	176.3235	-38.2917	0.2	-1.2	-12.0	0.5	0.6	1.2	1.2	0.6
3067	176.3291	-38.2640	-0.3	-2.4	-15.0	0.5	0.6	1.2	2.4	0.6
3077	176.4283	-38.3051	-1.7	-3.4	-6.8	0.5	0.6	1.2	3.8	0.6
3078	176.4598	-38.3112	-0.7	-4.7	-3.4	0.6	0.7	1.3	4.8	0.7
3079	176.5003	-38.3183	-0.6	-5.5	-10.7	0.5	0.6	1.2	5.5	0.6
3080	176.5017	-38.2776	-1.2	-5.2	-4.2	1.0	1.2	4.3	5.3	1.2
3081	176.3881	-38.3192	-1.3	-3.4	-3.4	0.5	0.6	1.2	3.6	0.6
3093	176.2983	-38.2335	1.8	-4.0	-8.1	0.5	0.6	1.2	4.4	0.6
3094	176.3207	-38.2492	-0.2	-4.0	-13.4	0.5	0.6	1.2	4.0	0.6
6881	176.6847	-37.9821	-0.6	-6.7	1.7	1.9	2.2	7.2	6.7	2.2
A4K6	176.3932	-37.8628	0.1	-1.6	0.6	1.9	2.2	7.2	1.6	2.2
A7LF	176.7340	-38.3764	1.1	-9.3	-1.9	0.5	0.6	1.2	9.4	0.6
A7LJ	176.8272	-38.3757	-1.1	-10.4	-0.2	0.5	0.6	1.2	10.5	0.6
A86L	176.1690	-38.3140	3.7	-4.6	-9.1	0.5	0.6	1.2	5.9	0.6
A86T	176.2143	-38.3289	-0.3	-3.4	-12.4	2.1	2.5	9.6	3.4	2.5
A86W	176.1377	-38.3020	3.1	-4.2	-8.5	2.1	2.5	9.6	5.2	2.3
A87P	176.0179	-38.3596	2.2	-2.8	-4.5	2.1	2.5	9.6	3.6	2.3
A886	176.1582	-38.3643	3.5	-6.1	-12.3	2.1	2.5	9.6	7.0	2.4
A88G	176.3007	-38.3376	0.0	-1.8	-10.3	0.5	0.6	1.2	1.8	0.6
A88H	176.2877	-38.3520	-1.1	-2.3	-9.3	0.5	0.6	1.2	2.5	0.6
A9BM	176.7371	-38.0765	1.2	-7.2	-0.7	0.5	0.6	1.2	7.3	0.6

Table 2. (Continued.)

Site	Long.	Lat.	V_E	V_N	V_{UP}	σ_{VE}	σ_{VN}	σ_{VUP}	$ V_{hor} $	$\sigma_{ V_{hor} }$
AGB9	176.4878	-38.4725	-0.3	-7.6	0.8	1.3	1.5	4.1	7.6	1.5
AGUG	176.5345	-38.0364	-0.8	-4.3	-1.0	0.9	1.0	2.2	4.4	1.0
AH9J	176.0301	-38.3875	4.3	-4.3	-5.3	1.9	2.2	7.2	6.1	2.0
B26Q	176.2547	-38.1689	2.9	-4.4	-8.7	0.5	0.6	1.2	5.3	0.6
B4DP	175.8775	-37.8943	-0.3	1.3	-0.8	1.0	1.1	2.7	1.3	1.1
B4HJ	176.2525	-38.1304	1.8	-4.7	-4.9	0.9	1.0	2.2	5.0	1.0
BE2T	176.3028	-38.4768	-2.4	-4.7	-9.1	0.5	0.5	1.0	5.3	0.5
BEVJ	176.0981	-38.4070	4.6	-4.5	-12.2	1.0	1.2	4.3	6.4	1.1
CBWR	176.7530	-38.2566	1.2	-9.3	1.8	0.5	0.6	1.2	9.4	0.6
CBWU	176.0813	-38.1529	0.6	-0.8	-0.8	0.6	0.7	1.5	1.0	0.7
CBWV	176.5608	-38.4079	0.3	-7.2	-1.4	0.7	0.7	1.6	7.2	0.7
CBWW	176.5220	-38.2292	-2.4	-3.4	-7.2	0.5	0.6	1.2	4.2	0.6
E4MH	176.1632	-38.4107	0.8	-4.3	-15.5	2.1	2.5	9.6	4.4	2.4
EAXX	176.1238	-37.8892	0.5	0.1	-2.1	1.9	2.2	7.2	0.5	1.9
EAXY	176.8194	-38.1136	2.0	-10.3	-1.0	1.9	2.2	7.2	10.5	2.2

resolution in this segment means our results add little insight to previous geological estimates of ground uplift or subsidence there. An exception is station RGMT, near the Bay of Plenty (see Fig. 1), where an uplift of 10 mm yr^{-1} is observed.

In general, horizontal velocities in the OVC region (Fig. 4) show a subtle variation in direction southwards through the caldera. This is most pronounced through the Tarawera volcanic complex (particularly near the Tarawera Rift and geothermal fields south of the OVC) where we observe a more rapid clockwise rotation. With the exception of station RGMK, little change in horizontal velocity rate occurs alongside these rotations. We also observe a broad pattern of subsidence in this area and increased subsidence rates in the geothermal areas south of the OVC (see Figs 5 and 6). The sparse data at the intersection of the Okataina and Whakatane segments do not allow us to constrain deformation well in this region.

Outside and along the western boundary of the Kapenga segment (see Fig. 1) (e.g. near stations AH9JM, A87P and A86W), horizontal velocities are oriented perpendicular to the segment axis (trending southeast), between 3.6 and 6.5 mm yr^{-1} (see Fig. 4). This pattern extends northwards into the Rotorua caldera (e.g. station RGUT). Fig. 4 also shows that stations along the eastern side of the Kapenga segment (e.g. stations A88G, A88H and 2309) trend south to southwest at slower rates. Eastern Kapenga segment border faults (including the Paeroa fault) appear to define a kinematic boundary, which divides southeast trending velocities within the TFB from the southerly or southwesterly motions east of the rift (see Fig. 4). The horizontal deformation field described by these velocities suggest significant contraction within this segment. We discuss this in more detail in the following section.

We identify a regional subsidence signal through the central rift, with rates varying from -4.5 to -15 mm yr^{-1} (see Figs 5 and 6). Exceptions include very large subsidence rates ($>-15 \text{ mm yr}^{-1}$) measured at station 2313 and RGHL. Excluding these exceptions, our subsidence pattern agrees well at a first order, with the pattern defined by precise levelling (Blick & Otway 1995). We have no GPS stations within the TRB but note that the precise levelling of Blick & Otway (1995) measure significant subsidence there too. We observe a localized and complex horizontal ground deformation pattern immediately southwest of the OVC in the vicinity of northern strands of the Whirinaki, Tumanui and Paeroa faults (see Fig. 2). Here, velocities decrease rapidly (from northwest to southeast) to only a few millimetre per year, alongside a pronounced clockwise rotation of their trend direction (see Fig. 4). Significant subsidence rates are also observed throughout this region.

Strain rates

We computed the areal strain rate through the study area using the velocities derived from the GPS position time series and the SSPX software (Cardozo & Allmendinger 2009). SSPX uses 2D (or 3D) horizontal velocity components to determine best-fitting strain tensors. Because of the spatially highly variable GPS network density, we opted to discretize the domain using a Delaunay triangulation instead of a regularly gridded domain. Each cell's nodes are GPS stations and an areal strain rate is computed for each cell. The triangulation approach allows some preservation of information in high network density areas while avoiding interpolation in sparse regions. One limitation of this approach is that spurious velocity values at a single station can substantially affect strain calculations for all adjacent cells. Caution must therefore be exercised when interpreting individual local and maximum strain rates for given cells as those are best interpreted in the context of values at neighboring cells. The strain computation process can be summarized as first solving a set of linear equations for the displacement gradient tensor G_{ij} and then compute the Lagrangian strain tensor E_{ij} . Finding the principal strain components equates to compute the eigenvalues and eigenvectors of E_{ij} . The reader is referred to Cardozo & Allmendinger (2009) and Means (1976) for more detailed information about strain computation.

Horizontal principal strain rates are shown in Fig. 7. The estimated dilation and maximum shear strain rates are illustrated in Figs 8 and 9 respectively. In general, the main features of the principal strain rate field are lower strain rates (less than approximately $0.2 \times 10^{-6} \text{ yr}^{-1}$) outside the Taupo Rift (both NW and SE of the rift) and increased (up to approximately $1.5 \times 10^{-6} \text{ yr}^{-1}$) and more variable rates within the Taupo Rift, particularly within the Kapenga and Okataina segments. In the west and northwest of the study region, lower rates are evident in the maximum principal strain rate axes (see Fig. 7). Fig. 7 also suggests extensional strain rates ($0.2\text{--}0.4 \times 10^{-6} \text{ yr}^{-1}$) along much of the eastern border of the Kapenga segment extending into the Rotorua caldera. Shear strain rates are also lower (relative to those within the rift) along this region (see Fig. 9) and the directions of the maximum principal strain rate axes are rift orthogonal. Some shear strain rates are also observed in the southwest of the Rotorua caldera. Across the Kaingaroa plain, lower strain rates are observed (approximately $0.2 \times 10^{-6} \text{ yr}^{-1}$) and the directions of maximum principal strain rate axes are rift orthogonal.

The most striking aspects of the horizontal strain rate field through the central rift are (1) the presence and localization of

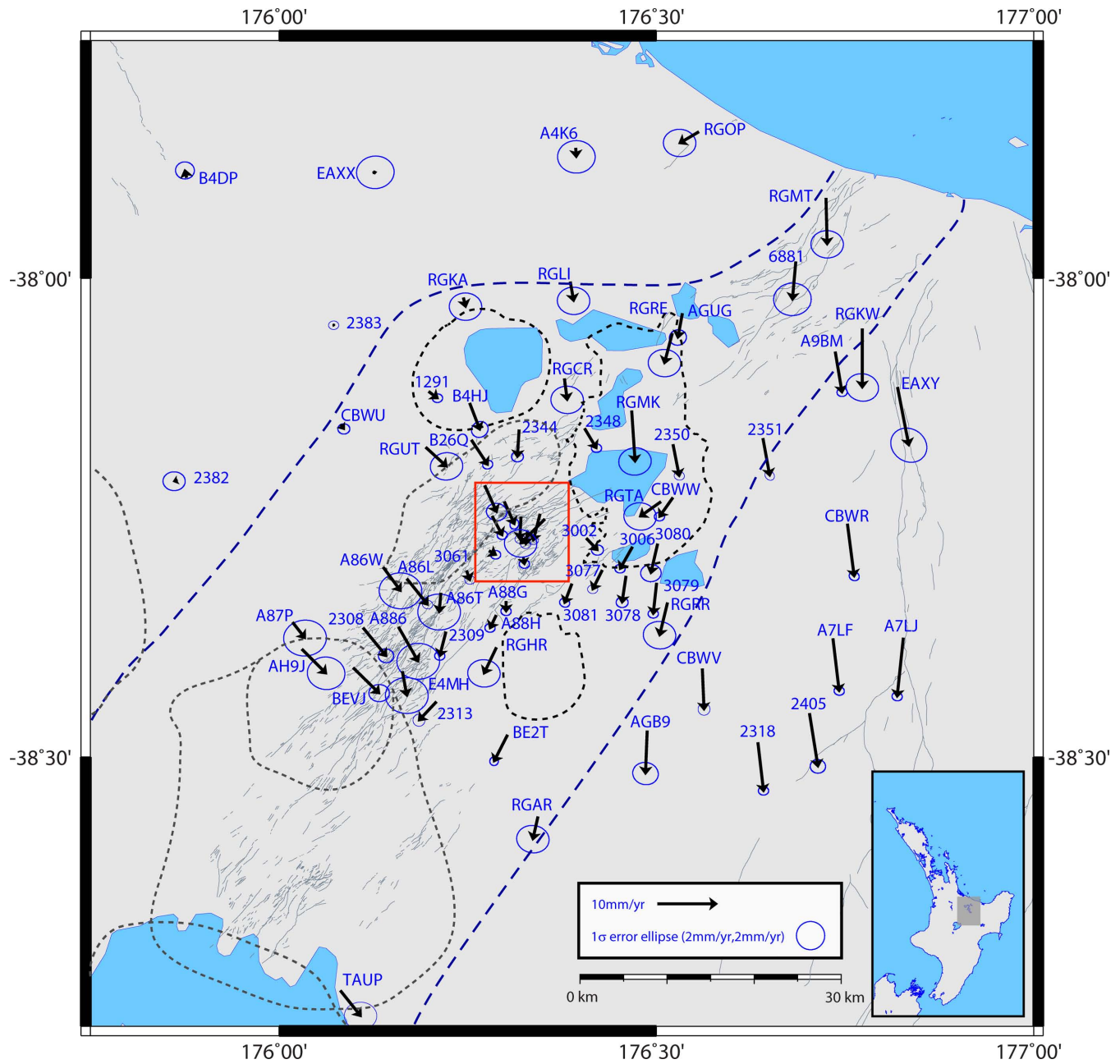


Figure 4. Horizontal GPS velocities in the local fixed reference frame, defined by campaign stations west and northwest of the rift (see the text for further details). Locations of calderas are shown as dashed grey lines and are approximate. Red inset same as Fig. 3. Dashed blue lines represent approximate location of modern rift boundaries. Bottom right inset show location of study area.

significant shortening rates within and along the Kapenga segment (see Fig. 7) and (2) the strong contrast of this contraction to the elevated horizontal extension strain rates near the Tarawera Rift. Shortening within the Kapenga segment is localized to a narrow zone coinciding with the Ngakuru, Maleme and Whirinaki fault zones (see Fig. 2). Shortening rates here are remarkably uniform in magnitude (approximately $-1 \times 10^{-6} \text{ yr}^{-1}$) and the direction of the minimum strain rate axes trends rift perpendicular. Strain rates through the OVC and its vicinity are not uniform in rate or orientation. In general, significant shortening is measured in the Haroharo complex (trending N-S) and elevated extension through the Tarawera Dome Complex and south through Lake Rotomahana (see Fig. 2). The largest principal strain rate we observe in the

Tarawera Rift is approximately $1.5 \times 10^{-6} \text{ yr}^{-1}$, trending rift orthogonal. The magnitude of this strain rate is large, but matches that estimated by Scott (1989). We also determine elevated positive dilation (between approximately 0.5 and $1.5 \times 10^{-6} \text{ yr}^{-1}$) and significant shear strain rates through the Tarawera Rift and negative dilation (compression) across Lake Tarawera. South of the OVC, at the intersection of the Kapenga segment, we also observe elevated amounts of horizontal shear (see Fig. 9), which appears to occur along much of the length the Paeroa fault leading towards the OVC.

Although we have sparser distribution of data across the Whakatane segment, lower and more uniform strain rates are observed there. We also find anomalous minimum principal strain rates in the vicinity of stations RGKW and A9BM (see Fig. 3) whose axes

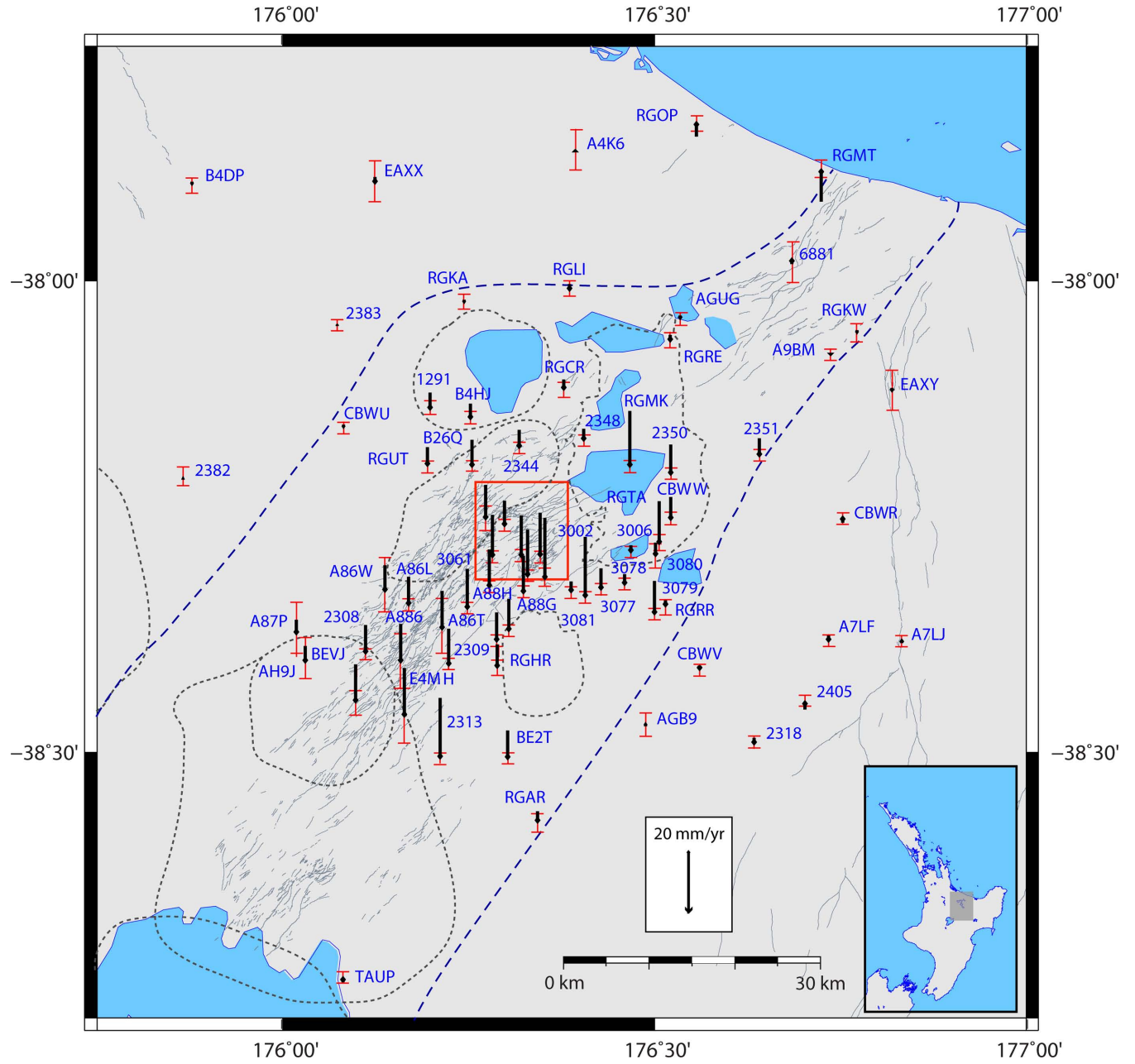


Figure 5. Vertical velocities for GPS stations in the local fixed reference frame. Vertical error-bars indicate 68 per cent standard deviation. Light black lines are active rift faults from the GNS Science Active Faults Database. Locations of calderas are shown as dashed grey lines and are approximate. Red inset same as Fig. 3. Dashed blue lines represent approximate location of modern rift boundaries (Acocella *et al.* 2003). Bottom right inset shows location of study area.

are closely aligned with the rift segment axis. They most likely reflect poor geodetic resolution through this region, as well as poor spatial sampling in the Delaunay triangulation. Some shear strain rates are also modelled through this region, which might be related to shortening identified there. No significant dilation (relative to within the rift) is evident in this region (see Fig. 8).

Geodetic strain rates determined from the SSPX software provide a good insight into spatial patterns of extension and contraction through horizontal velocity fields. This approach can, however, be influenced by velocity uncertainties (for 3 node Delaunay triangulation) and geometry effects (e.g. averaging effects) (Serpelloni *et al.* 2006). Following Vigny *et al.* (2007), Payne *et al.* (2012) and Kogan *et al.* (2012), we generate horizontal GPS velocities profiles

(see Fig. 11) to estimate strain rates across the study area without the geometry effects of SSPX triangulation. To do this we project our horizontal velocities onto 2D profiles orthogonal (trending 120 deg) to the inferred rift axis (30 deg E from Acocella *et al.* 2003). As these transects are perpendicular to the inferred rift axis, they allow us to estimate rift perpendicular strain rates across the study area (see Fig. 10). We fit a surface through these rift-perpendicular velocities to examine patterns of rifting through the study area. We then produce velocity profiles through the Whakatane, Okataina and Kapenga segment (see Figs 11a–c). Using least-squares linear regression we also determine strain rate estimates from velocity gradients in these figures (dark green lines and text in Fig. 11). Positive slopes therefore reflect extension and negative slopes shortening.

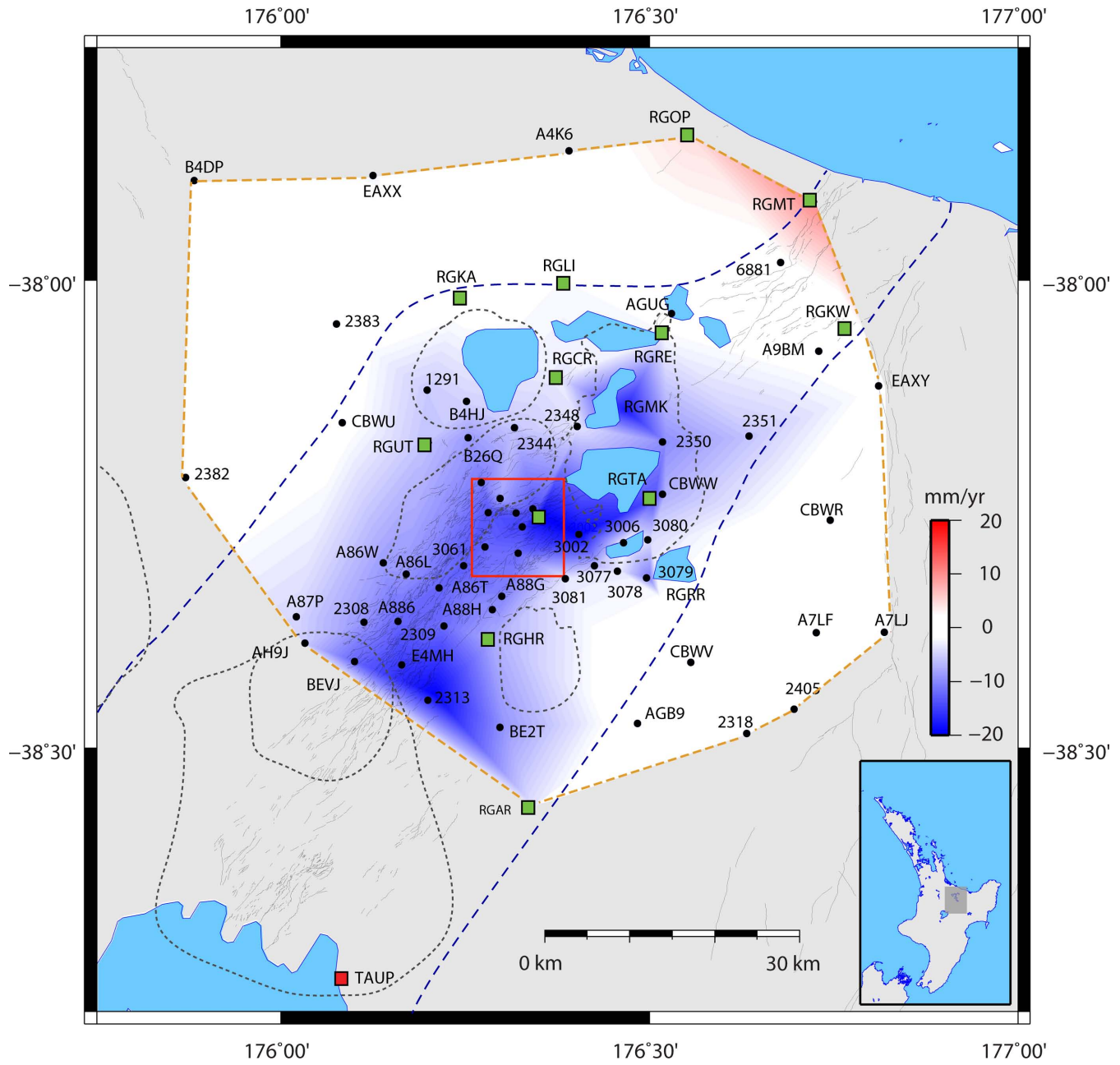


Figure 6. Fitted surface of vertical velocities through the study area (produced using Triangulate command in GMT). Color-coded scale for velocities is included at bottom right. Dashed orange lines represent limit of triangulation modelling. Dashed blue lines represent approximate location of modern rift boundaries (Acocella *et al.* 2003). Caldera boundary locations are shown as dashed grey lines are approximate. Red inset same as Fig. 3. Bottom right inset shows location of study area.

Fig. 11(a) suggests a rift-perpendicular extension rate across the Whakatane graben of 4.5 mm yr^{-1} . A maximum rate of 7 mm yr^{-1} is measured in the vicinity of the AXIR tectonic block. The velocities across the Whakatane graben show an estimated strain rate of $0.24 \pm 0.08 \times 10^{-6}$ (estimated over approximately 17 km distance). However, if we consider the 2 mm yr^{-1} velocity of station RGOP away from the rift axis, our total rifting estimate across the Whakatane profile is 9 mm yr^{-1} . This compares well with the geodetic estimate of Walcott (1987) of 12 mm yr^{-1} but less than that predicted by Wallace *et al.* (2004) of 15 mm yr^{-1} , although we note that their total extension rate was for the North Island forearc relative to the Australian Plate.

Rift-perpendicular extension rates across the Okataina profile are varied (Fig. 11b). We do not attempt to determine a single regression estimate there, due to the heterogeneous nature of these velocities and the possible influence of transient velocities within the caldera. In general, extension increases from east to west, where we observe a maximum rate of 5.5 mm yr^{-1} toward the AXIR tectonic block. However, locally increased velocities are observed near the Rotorua and Haroharo caldera (4 and 5 mm yr^{-1} respectively). Fig. 11(b) also shows decreased horizontal velocities in the vicinity of the Tarawera Rift, which could be interpreted to indicate contraction there. However, we consider this an artifact of projecting the locally rotated horizontal velocities in the Tarawera Rift onto the Okataina

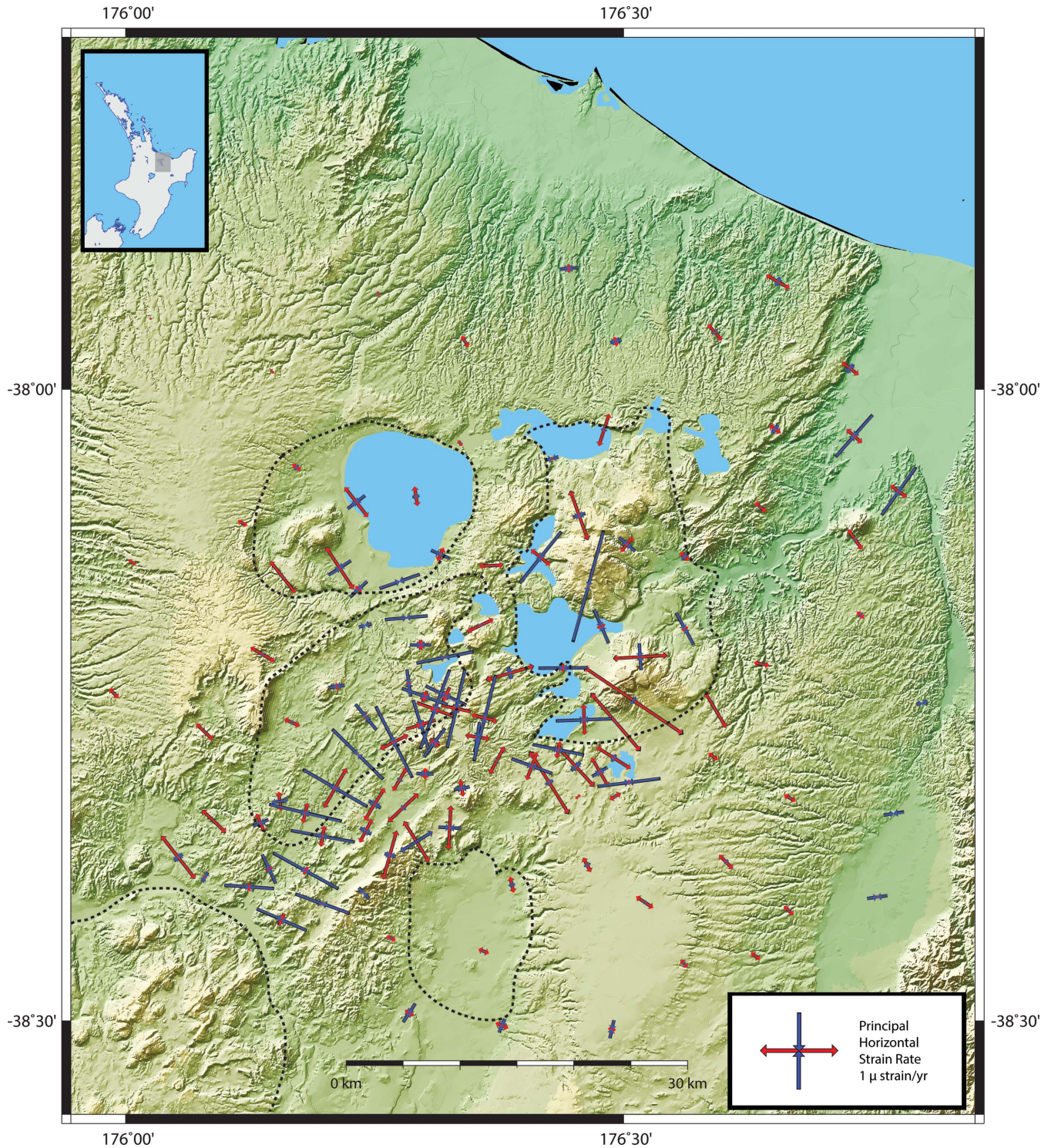


Figure 7. Horizontal principal strain rate axes derived from horizontal GPS velocity rate estimates using the Delaunay approach in SSPX software (Cardozo & Allmendinger 2009). Caldera boundary locations are shown as dashed black lines and are approximate. Top left inset shows location of study area.

line profile. We also note that the projected velocities in Fig. 10, do not account for rift segment axis variations, particularly through the Okataina segment, which has a more easterly orientation than neighboring segments. For these reasons, the use of 2D velocity profiles to estimate strain rates across this part of the Taupo Rift may be limited.

Estimates of rift related extension across the Kapenga profile must also be made with caution due to the probable influence of magmatic or hydrothermal processes there. The velocity profile shown in Fig. 11(c) reflects this. However, orthogonal extension across this profile appears to be focused immediately west of the TVZ (see Figs 4 and 11c). In this region velocities rapidly increase eastwards,

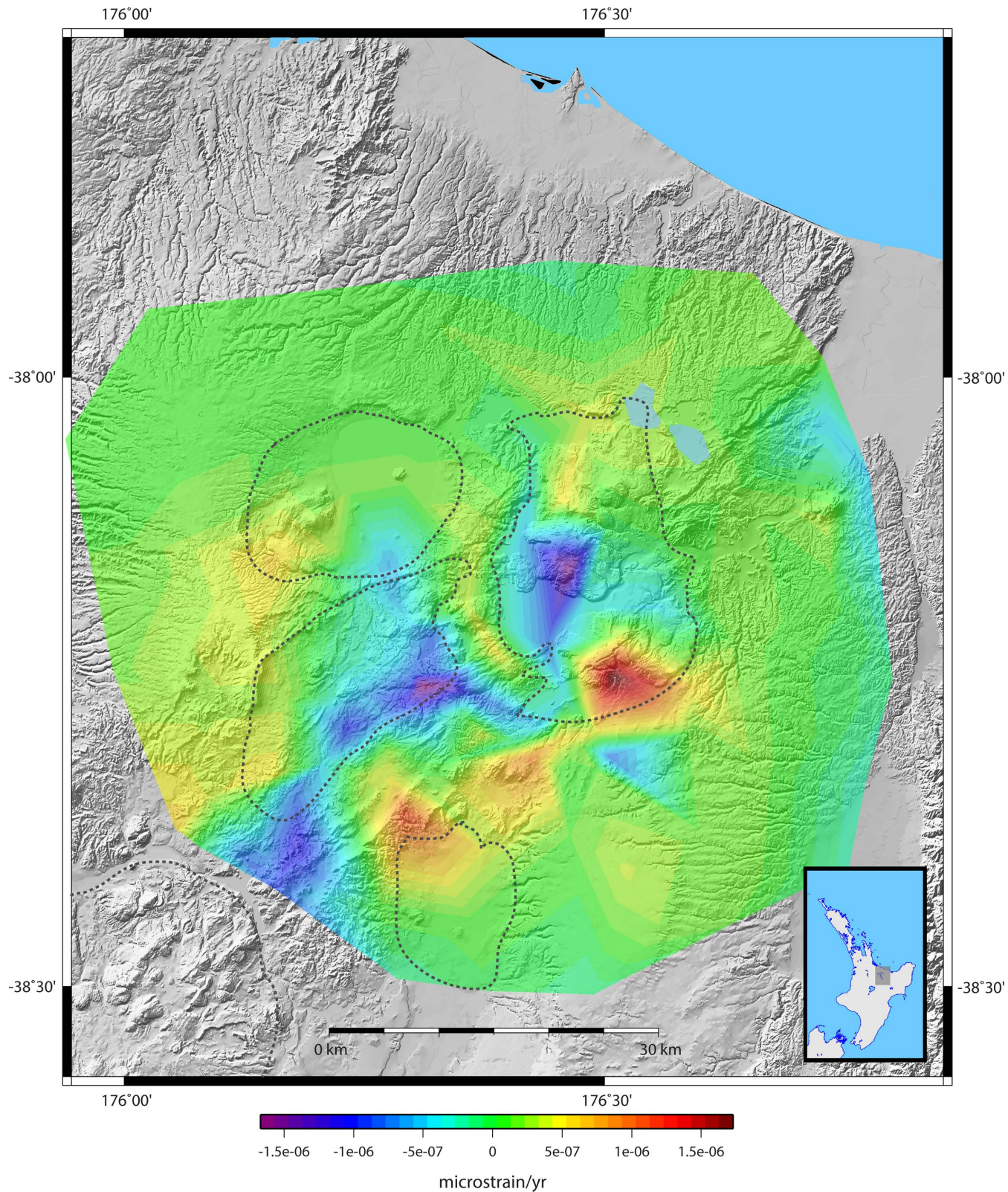


Figure 8. Dilation strain rate field derived from horizontal GPS velocity rate estimates using the Delaunay approach in SSPX software (Cardozo & Allmendinger 2009). Caldera boundary locations are shown as dashed grey lines and are approximate. Bottom right inset shows location of study area.

and then abruptly decrease east of the central axis. The estimated strain rate (determined from the profile velocity gradient) here is $0.20 \pm 0.1 \times 10^{-6}$ (estimated over approximately 27 km distance). Across the central axis of the Kapenga segment, the faster south-

east velocities west of the axis, compared to the slower southerly motions along the eastern side suggest shortening between the Ngakuru graben to the Paeroa fault zone of 6 mm yr^{-1} . A shortening strain rate of $-0.99 \pm 0.08 \times 10^{-6}$ (estimated over approximately

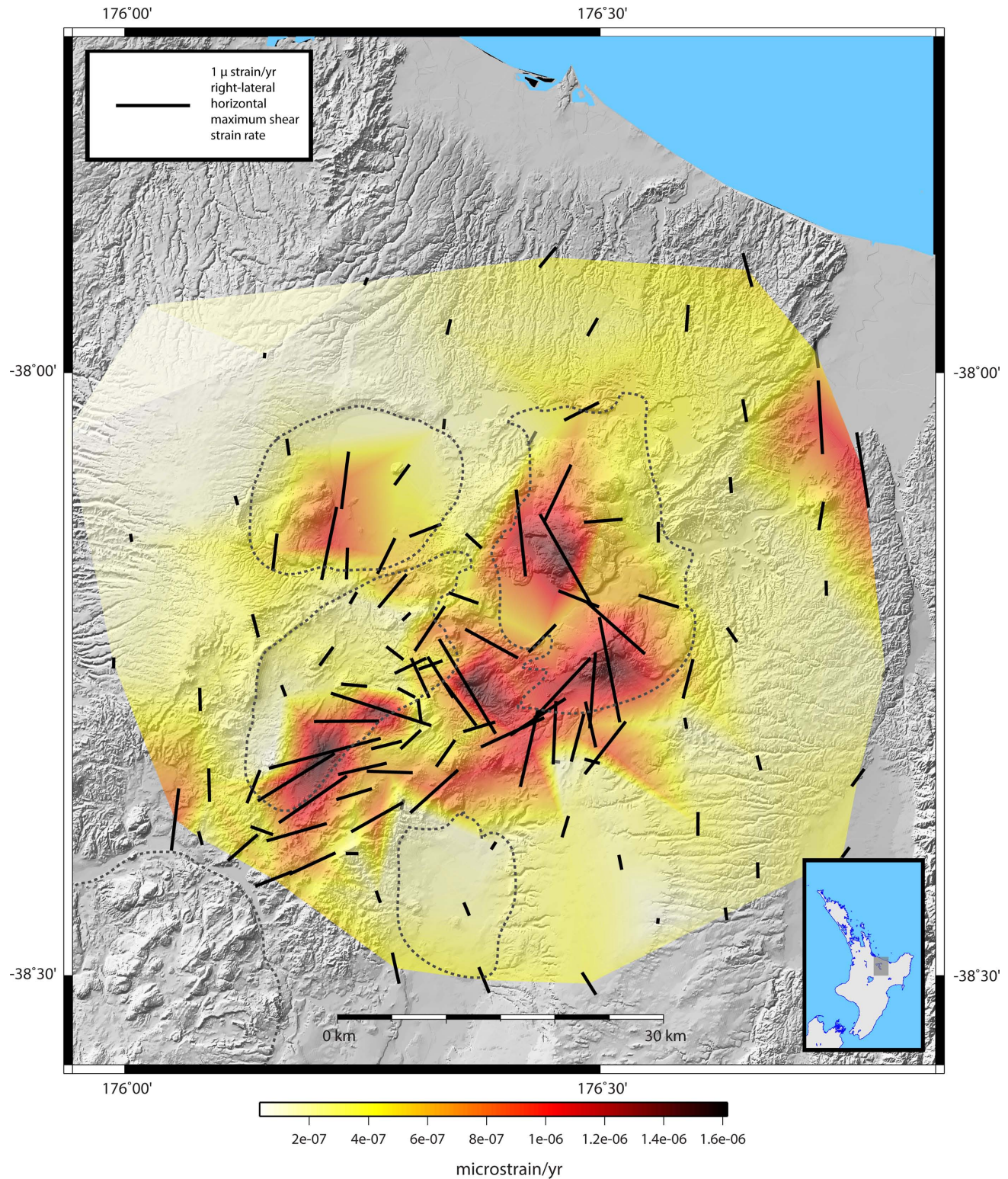


Figure 9. Shear strain rate field derived from horizontal GPS velocity rate estimates using the Delaunay approach in SSPX software (Cardozo & Allmendinger 2009). Shear strain rate lines are right lateral. Caldera boundary locations are shown as dashed grey lines and are approximate. Bottom right inset shows location of study area.

10 km distance) is estimated for this section of the profile. This shortening observed in the GPS is at odds with the longer-term extension observed on the Paeroa fault and Ngakuru Graben (Villamor & Berryman 2001, 2006), suggesting that is related to non-tectonic (e.g. volcanic and/or magmatic) processes. East of the Re-

poroa caldera and across the Kaingaroa plain, velocities increase suggesting extension rates of approximately 3.5 mm yr^{-1} . An extension rate of $0.13 \pm 0.012 \times 10^{-6}$ (estimated over approximately 22 km distance) is derived for this section of the Kapenga velocity profile.

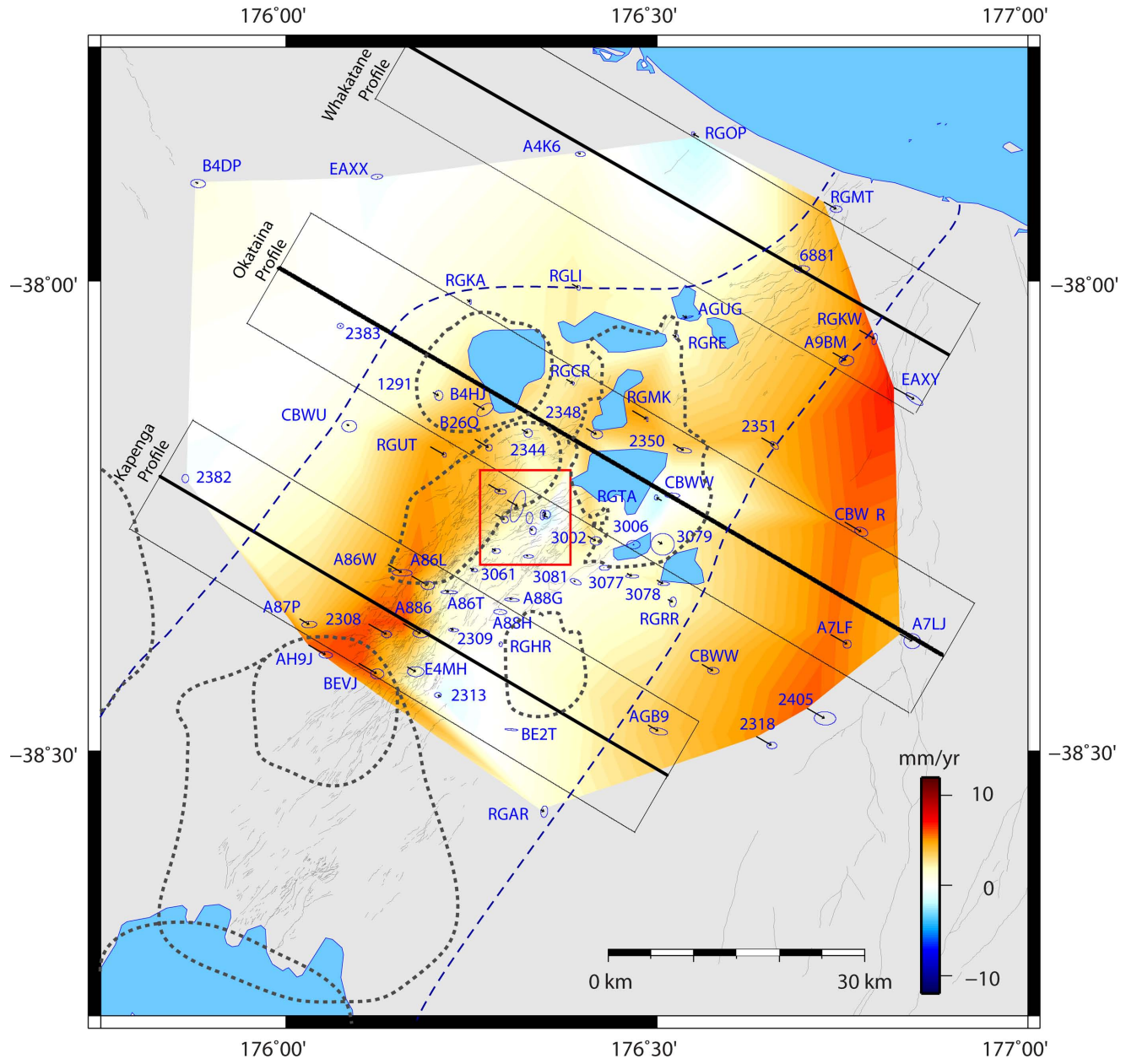


Figure 10. Fitted surface to orthogonal velocities across the study site (produced using Triangulate command in GMT). Dashed blue lines represent approximate location of modern rift boundaries (Acocella *et al.* 2003). Caldera boundary locations are approximate.

INTERPRETATION OF RESULTS ACROSS THE STUDY AREA

Outside the rift

The horizontal strain rates across the study area show a distinction between lower rates (outside the Taupo Rift), compared with higher rates (both extension and shortening) within the rift. We interpret this to differentiate deformation processes related to magmatic and tectonic deformation within the rift from regional deformation processes outside the rift. Strain rates outside the rift are typically smaller than 0.2×10^{-6} , while those within the rift are larger and can be up to (on average) approximately 1 to 1.5×10^{-6} . This distinction is also visible in the vertical velocities (see Figs 5 and 6), although to a lesser degree in the Whakatane graben. We find that our strain rate estimates outside the rift are in good agreement with

that of Darby *et al.* (2000), who estimate strain rates of 0.21×10^{-6} across a similar region. The strain rate identified using regression in Fig. 11 is also similar to their estimate. However, their strain rate estimate is based on data with a much lower spatial resolution and as such we cannot compare results in greater detail.

Outside the rift, we can link our results to a number of regional tectonic structures or magmatic processes. First, we locate the tectonically stable western North Island, northwest of the Taupo Rift, based on the coherent horizontal and vertical motion observed in this region. Second, we consider the coherent horizontal motions, decreased vertical velocities and increased extension in the east and southeast of the study area to be linked to clockwise rotation of the AXIR block (Wallace *et al.* 2004). Lower strain rates east of the Paeroa fault may also reflect background tectonic processes and structure, as the magnitude of strain rate in this region is

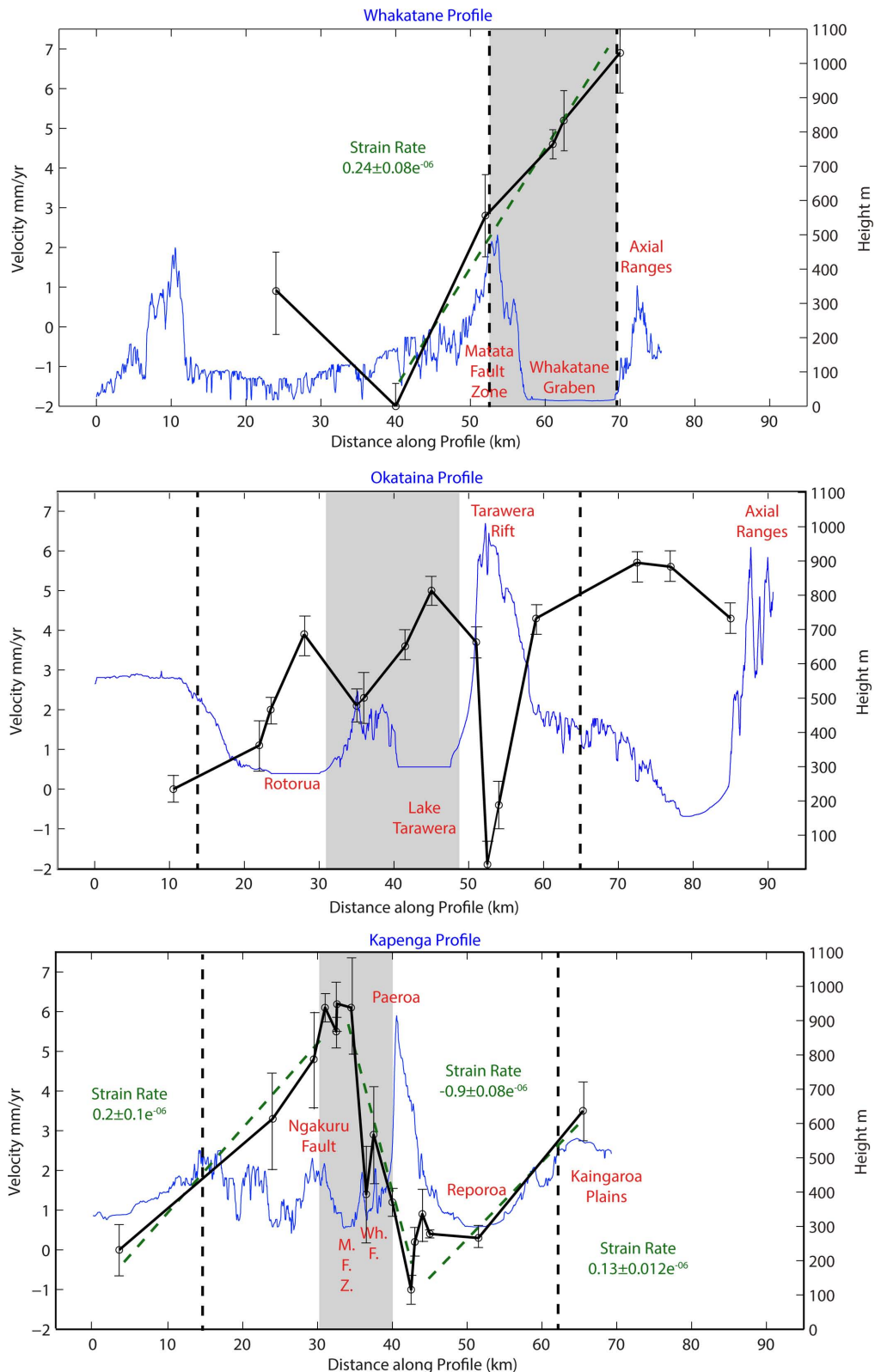


Figure 11. Velocity profiles produced for (a) Whakatane, (b) Okataina and (c) Kapenga segments (black lines) from plotting velocity components orthogonal to rift segments (in millimetre per year) as a function of distance (in kilometres). Error-bars indicate 68 per cent standard deviation. Solid black lines represent interpolated horizontal velocity between stations in each profile. Green dashed lines represent best-fit horizontal velocity estimates using least-squares regression approach for different sections of profile. The strain rate values associated with each estimate are shown in green text. The topography of each profile is also overlain as blue lines. Dashed vertical lines represent the approximate location of the TVZ boundaries. Caldera boundary locations are approximate. Grey shaded area represents the approximate location of rift-related normal faulting.

significantly less than that within the Taupo Rift. The Paeroa fault is a major rift scale structure, with a fast slip rate and no common recurrence interval (Villamor *et al.* 2008). Our results suggest that the Paeroa fault zone might play an important role in controlling deformation in this part of the rift and, geodetically at least, may delineate an eastern boundary of rift related deformation in this region, despite the fact that we currently observe contraction in the region of this fault. Magnetotelluric data indicate that shallow melt may exist just below and east of the Paeroa fault (Bertrand *et al.* 2012). Contraction in the central rift has been linked to magma cooling (Hamling *et al.* 2015) and it is likely that the strain rate pattern we observe through this region reflects this. A similar association may also explain the lack of significant surface deformation we observe in our geodetic data across the Reporoa caldera (and vicinity). The results there do not provide evidence to confirm that significant extension is currently accommodated across the TRB as proposed by Rowland *et al.* (2010).

Inside the rift

In general, we interpret the high rates and broad scale subsidence rates within the rift to delineate the zone of active deformation related to rifting. The $2\text{--}3\text{ mm yr}^{-1}$ extension rate decrease between the Whakatane and central segment agrees with that predicted in the wedge-shaped extension model of Wallace *et al.* (2004). This supports tectonic block rotation along the eastern North Island as a regional mechanism for driving rifting in the Taupo Rift (Wallace *et al.* 2004). However, within the Kapenga and Okataina segments, subsidence rates are too large to be linked purely to rifting and it is likely that hydrothermal or magmatic system processes contribute significantly. This is reflected in the highly heterogeneous horizontal strain rate and velocity fields in the Kapenga and Okataina segments we identify, which are difficult to link to an individual source. For instance, the significant change in orientation of the principal strain rate axis between the Kapenga (contraction) and the Okataina segment (i.e. extension at the Tarawera Rift) (see Fig. 7) could be interpreted as geodetic evidence to support a variation in rift structure. However, such heterogeneity is likely related to transient deformation from magmatic and hydrothermal activity, particularly at this location in the rift, where magma emplacement into the upper crust is considered possible.

Only in the Whakatane graben, can we confidently interpret strain rates and velocities to reflect rift-perpendicular extension. Our extension rate there of 9 mm yr^{-1} using GPS is less than that predicted by Wallace *et al.* (2004). We attribute this difference to our measurements not sampling the entire AXIR tectonic block, which they use in their modelling. However, we associate the coherent pattern of gradually increasing velocities towards the AXIR tectonic block to clockwise rotation of this block. We interpret the local uplift signal observed at station RGMT to be linked to seismicity and fault movement in the Matata Fault Zone (Wright 1990; Beanland & Haines 1998; Mouslopoulou & Hristopulos 2011).

Within the OVC

Interpreting the results in the OVC is more difficult and requires caution due to the OVC's location within both a rift setting and an active caldera. In general we associate the highly heterogeneous strain rates and velocity field to either regional tectonic and/or local magmatic processes. For example, the broad scale clockwise rotation of horizontal principle strain rate axes across the caldera

(see Fig. 7) could be linked to rift structure variation. The more localized elevated strain rates along the Tarawera Rift (and vicinity) we interpret to either tectonic or possibly volcanic origin, which we discuss in the following section. We attribute the large subsidence rates across Lake Tarawera, Lake Rotomahana, south of the OVC, as related to active magmatic and/or hydrothermal subsidence. Such large rates are not unusual and have been documented in other hydrothermal areas within the rift (Allis *et al.* 2009; Bromley *et al.* 2009).

DISCUSSION

Processes driving contemporary deformation in the Taupo Rift and OVC

Our results constrain the pattern of ground deformation through the central rift in greater detail than previous studies using GPS data and indicate that it is not uniform in rate or distribution. This is indicated by the presence of a number of remarkable features, which include (1) significant contraction within the Kapenga segment and extension offset westwards from the zone of normal faulting, (2) rapid changes of principle strain rate axis orientations at the intersection of the Kapenga and Okataina segments, (3) elevated extension and shear strain rates at the Tarawera Rift within the OVC, (4) very large subsidence rates in the central rift (up to -1.94 cm yr^{-1}) and (5) lower extensional strain rates than previously documented in the Whakatane graben (Wallace *et al.* 2004).

It is not clear why we observe contraction within the normal fault system of the Ngakuru graben and Paeroa fault, and extension up to approximately 15 km west of the main rift axis. A similar pattern was also observed north and northwest of Lake Taupo (30 km south of our study region) by Darby *et al.* (2000) using GPS data from 1986 to 1997. This pattern does not agree with abundant geological estimates of normal faulting in the central rift. Hamling *et al.* (2015) link the large subsidence rates in this part of the rift to cooling of large-scale magma bodies at approximately 6 km depth. A magma cooling mechanism would explain the mismatch we observe between contemporary contraction from our GPS data and the long-term geological estimates in that region. This would suggest that present day magmatic processes are masking geological observations of long-term normal faulting in the Kapenga segment and are also responsible for the observed extension west of the main rift axis. Subsequently, in this part of the rift we cannot confidently link ground deformation patterns to upper crustal faulting from our geodetic data.

The deformation pattern at the intersection of the Kapenga and Okataina segments (and the southwestern border of the OVC) is the most complex in the study area. This includes significant principle strain rate axis rotations (up to tens of degrees) (see Fig. 7), elevated shear strain rates (approximately 1 to $1.4 \times 10^{-6}\text{ yr}^{-1}$) (see Fig. 9) and large vertical velocities (up to -1.97 cm yr^{-1}). This heterogeneity could accommodate the extension rate decrease we observe southwards through the rift and/or the proposed bend in rift architecture across the Okataina segment (Rowland & Sibson 2001; Acocella *et al.* 2003; Seebeck & Nicol 2009; Rowland *et al.* 2010; Seebeck *et al.* 2010). However, the subsidence rates are greater than those expected from rifting processes alone and it is more likely that magmatic processes contribute significantly. This conclusion is supported by the good agreement between our principle strain rate axes rotations and those modelled just south of Okataina by Ellis *et al.* (2014). They model clockwise rotations of extension axes due

to the presence of a large accumulation of partial melt orientated NW-SE south of Okataina. The elevated levels of upper crustal seismicity and the highly energetic hydrothermal fields in this part of the rift would suggest that our deformation field may also reflect a transition between different sets of hydrothermal and/or magmatic processes. Similar associations are often attributed to hydrothermal fluid pressurization and movement at other large caldera systems, including Taal (Lowry *et al.* 2001; Bartel *et al.* 2003), Campi Flegrei (Battaglia *et al.* 2006) and Yellowstone caldera (Puskas *et al.* 2007).

To the north of the OVC (in the Whakatane graben), we observe horizontal velocities similar to those in the AXIR tectonic block (see Fig. 4). Other than a small step change in velocity rates, there is little geodetic evidence of a significant discontinuity between the Whakatane segment and AXIR tectonic block. Also, the vertical velocities do not yield evidence for such a boundary. We consider this good evidence in support of the non-rotational strike-slip fault termination model of Mouslopoulou *et al.* (2007). A key component of their model is that the 4 mm yr⁻¹ strike slip transferred into the Taupo Rift in the Whakatane segment from the NIDFB occurs without any block rotation at the terminating faults (e.g. at the western side of the Whakatane graben). Our horizontal velocities show no evidence of such rotations (at least on a scale larger than tens of kilometres). We consider that the small uniform increase in horizontal velocities across this region reflects the influence of rotation of the AXIR tectonic block. This would explain the increased dextral shear we observe across the Whakatane graben (in agreement with Acocella *et al.* 2003).

The intermittent nature of our campaign data only provides a snapshot of surface deformation between major eruptive and/or tectonic episodes in the Taupo Rift and makes it very difficult to identify transient ground deformation patterns. Given the plentiful supply of magma and presence of energetic hydrothermal fields in central Taupo Rift, it is unlikely that the GPS velocities and strain rate features we identify there are representative of long-term tectonic processes. Therefore to consider the temporal stability of our results, we analyse the de-trended daily position time-series plots of the cGPS sites within the study area (see Figs 3 and 12—also available at www.geonet.org.nz). They show evidence of transient ground deformation patterns for all cGPS stations, but in particular stations TAUP (within the Taupo caldera) and RGHL (at the intersection of the Kapenga and Okataina segments). Both stations undergo significant rapid uplift (TAUP) and subsidence (RGHL) over approximately 5 yr, as well as two more rapid displacement periods (highlighted in yellow in Fig. 12). Given the short term time period associated with these deformation features, we attribute their source to magmatic, or hydrothermal processes. This implies that the highly heterogeneous horizontal velocities and strain rates seen in the vicinity of station RGHL from our campaign data may also accommodate some shorter-term transient deformation patterns. Further, the uplift and subsidence deformation patterns concurrently measured at different parts of the central rift provides evidence that magmatic processes vary spatially within this region, in agreement with earlier studies (Manville & Wilson 2003; Rowland *et al.* 2010).

Relationship of OVC deformation to volcanic, hydrothermal and tectonic processes and implications for geodetic monitoring

The co-location of high extension and shear strain rates (see Figs 7 and 9) with the location of the most recent volcanic activity (at

the Tarawera Rift) supports a causal relationship between magmatic/volcanic processes and ground deformation at the OVC. This deformation pattern provides a highly suitable environment for dyke and magma emplacement in the upper crust and agrees well with the observed patterns of left stepping en-echelon dykes related to the 1886 Tarawera eruption shown in the geological record (Nairn & Cole 1981). Therefore, it is tempting to link the elevated extension and shear strain rates in this region as a local driver for the AD 1886 Tarawera eruption. However, our results do not indicate if this deformation is a response to or has encouraged magma localization (e.g. upper crustal dykes) in the Tarawera Rift.

The elevated extension and shear strain rates through the Tarawera Rift could also be interpreted to support propagation of the Whakatane graben axis into the OVC caldera (e.g. a tectonic driver of deformation in the OVC) (Spinks *et al.* 2005). A puzzling aspect of this interpretation is the absence of significant upper crustal seismicity (at least during our study period) associated with the elevated strain rates in the Tarawera Rift (see Fig. 1). This seismicity is also low in comparison to the southwest boundary of the OVC and within the Haroharo dome complex. Similar (poor) correlations between deformation and seismicity have also been observed at other large calderas, including Yellowstone (Puskas *et al.* 2007). We propose that extensional and shear strain rates through the Tarawera Rift are presently accommodated with little significant upper crustal seismicity. Given that upper crustal seismicity might not be relied upon solely for evidence of magma migration to the surface here, any ground deformation in this region must be interpreted with caution. Deformation patterns in the vicinity of the Tarawera Rift must be watched closely.

We cannot confidently identify a volcanic signal within our OVC deformation field from the campaign data for the study period. This is likely due to either (1) the contamination of any volcanic geodetic signal by local tectonic and/or hydrothermal processes within the caldera and/or (2) the poor temporal resolution of the campaign GPS data, which may not have detected transient deformation related to local volcanic and hydrothermal activity. Moreover, little evidence of significant transient deformation is evident in the cGPS time series of stations inside the OVC (RGRE, RGMK and RGTA—see Figs 3 and 12). Only at station RGHL south of the OVC, outside the caldera boundary, is there evidence for a local magmatic deformation signal (at the start of 2010, highlighted in yellow in Fig. 12).

It has been hypothesized that preceding an OVC eruption, broad subsidence and local uplift signals would be observed in the geodetic data in the far and near fields respectively. It is therefore prudent to consider if these signals might be discernable within the contemporary deformation field using GPS data. Considering the dominant subsidence signal in the central rift, we suggest that a broad subtle subsidence signal would be difficult to observe in regional campaign GPS data. Campaign GPS data is better suited for longer-term (e.g., several years or more) deformation studies of overall processes, rather than observing short-term transient deformation that often occurs within calderas. cGPS data are required for the latter. Given that no volcanic crisis has occurred since the installation of the cGPS receivers in the OVC, and the short time span of their operation, reconciling any modern transient behaviour detected there with geological observations in the rift remains difficult.

CONCLUSIONS

In this study we use new and existing campaign and cGPS data collected from 1998 to 2011 to measure contemporary deformation

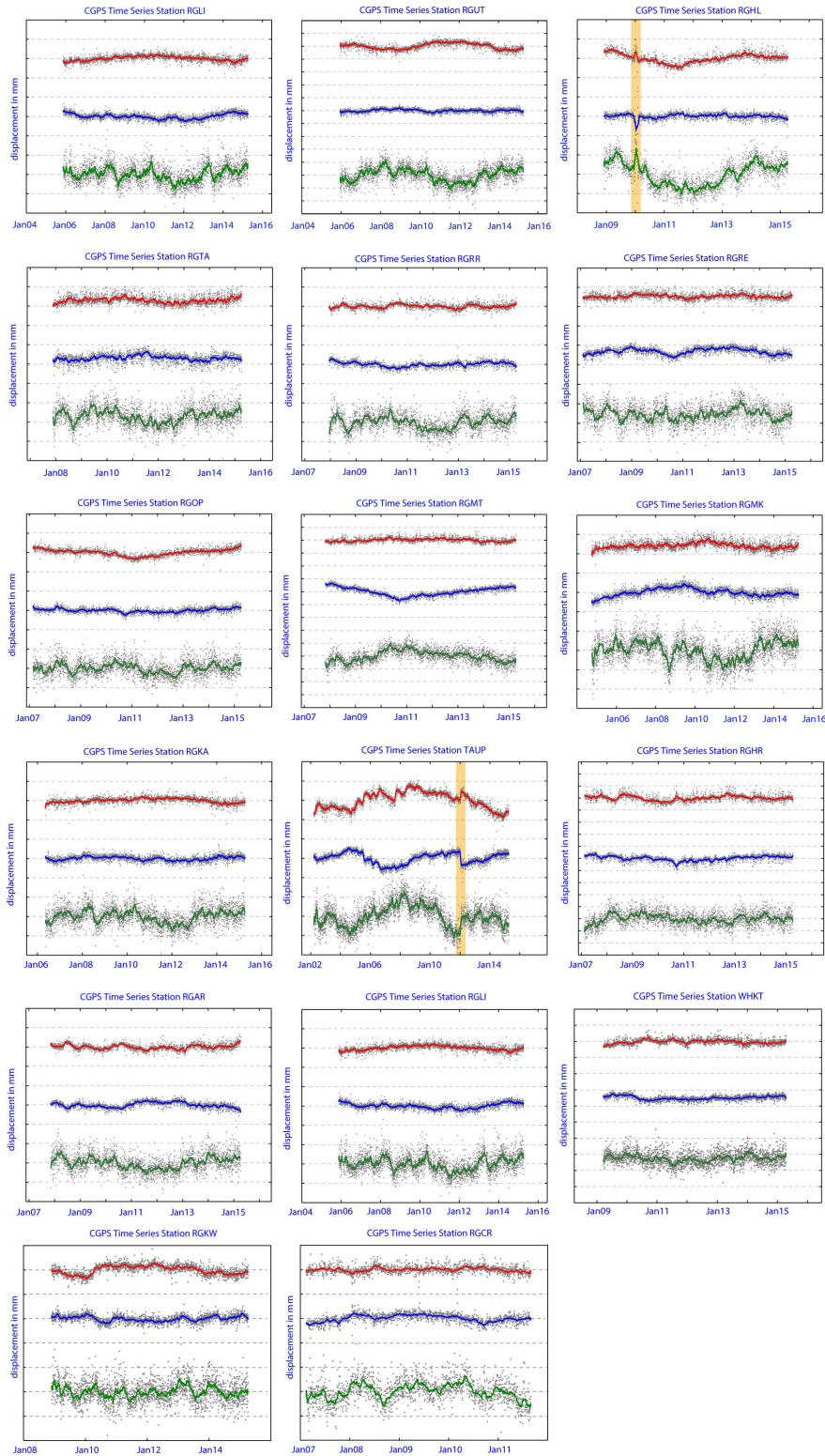


Figure 12. De-trended time series plots for cGPS stations with study region. The red, blue and green lines represent smoothed displacements from initial position in the easting, northing and height components respectively. Each time series has been offset for visual clarity. Spacing between grey horizontal grid lines in each plot represents 10 mm. Yellow vertical bands represent suspected transient displacement episodes at stations RGHL and TAUP. See Fig. 3 for station locations. Information regarding the removal of the regional signal from the data is available at the GeoNet webpage.

within the Taupo Rift and OVC. These results identify a heterogeneous velocity and strain rate field through the study area. We find a good agreement with existing geodetic estimates of extension rates in the study area. The major new contributions presented in this

paper include (1) the identification of large contraction within a large portion of the central Taupo Rift, which has not been previously highlighted or recognized, (2) revised rates of rifting in the Whakatane area, which appear to be slightly slower than in

previously presented (Wallace *et al.* 2004), (3) a detailed description and presentation of variations in crustal kinematics in the Okataina caldera, and its relationship to magmatic and tectonic processes and (4) the first published strain and velocity field for the TVZ from a comprehensive GPS data set.

In the central rift, we consider the contemporary deformation patterns to be dominated by magmatic sources. As a result, we observe a significant mismatch between the well-documented long-term geological estimates of fault movements (e.g. extension related to normal faulting in the central rift) with those predicted from our GPS velocities, as the current high GPS shortening rates may reflect cooling of a magma body (e.g. Hamling *et al.* 2015). As a result areas currently showing contraction from GPS (e.g. in the Ngakuru graben) probably shift to extension in the long term. While, areas undergoing extremely rapid subsidence through the central rift may be buoyed up by magma in the longer term and shift to uplift as magma migration patterns change. The Whakatane graben is the only location that may be appropriate for comparisons between the GPS and geological deformation rates, where the contemporary deformation patterns from GPS are in good agreement with those expected from geological studies.

In the OVC, we find no clear evidence of active volcanic processes. However, in the Tarawera Rift we identify a strain rate environment highly suitable for magma migration and dykes though the upper crust. We are unable to confidently determine if this is related to volcanic and magmatic processes, given the nearby hydrothermal activity and likely influence of regional tectonic structure. However, given the recent history of volcanism in this part of the OVC, future deformation there must be interpreted cautiously. Our results therefore provide a useful baseline study from which any local volcanic signals might be compared in the future.

ACKNOWLEDGEMENTS

This paper is dedicated to John Beavan whose generosity and willingness to discuss and assist in any aspect of the geodetic processing and interpretation of TVZ deformation will always be appreciated. All figures (except Figs 11 and 12) were produced using *Generic Mapping Tools* software (Wessel & Smith 1998). We thank the two anonymous reviewers for their comments which significantly improved this paper.

REFERENCES

- Acocella, V., 2010. Coupling volcanism and tectonics along divergent plate boundaries: collapsed rifts from central Afar, Ethiopia, *Bull. geol. Soc. Am.*, **122**(9–10), 1717–1728.
- Acocella, V., Spinks, K., Cole, J. & Nicol, A., 2003. Oblique back arc rifting of Taupo Volcanic Zone, New Zealand, *Tectonics*, **22**(4), 1045, doi:10.1029/2002TC001447.
- Allis, R., Bromley, C. & Currie, S., 2009. Update on subsidence at the Wairakei-Tauhara geothermal system, New Zealand, *Geothermics*, **38**(1), 169–180.
- Bartel, B.A., Hamburger, M.W., Meertens, C.M., Lowry, A.R. & Corpuz, E., 2003. Dynamics of active magmatic and hydrothermal systems at Taal Volcano, Philippines, from continuous GPS measurements, *J. geophys. Res.-Solid Earth*, **108**(B10), 2475, doi:10.1029/2002JB002194.
- Battaglia, M., Troise, C., Obrizzo, F., Pingue, F. & De Natale, G., 2006. Evidence for fluid migration as the source of deformation at Campi Flegrei caldera (Italy), *Geophys. Res. Lett.*, **33**(1), L01307, doi:10.1029/2005GL024904.
- Beanland, S. & Haines, J., 1998. The kinematics of active deformation in the North Island, New Zealand, determined from geological strain rates, *N. Z. J. Geol. Geophys.*, **41**(4), 311–323.
- Beavan, J., 2005. Noise properties of continuous GPS data from concrete pillar geodetic monuments in New Zealand and comparison with data from U.S. deep drilled braced monuments, *J. geophys. Res.-Solid Earth*, **110**, B08410, doi:10.1029/2005JB003642.
- Beavan, J. & Haines, J., 2001. Contemporary horizontal velocity and strain rate fields of the Pacific-Australian plate boundary zone through New Zealand, *J. geophys. Res.-Solid Earth*, **106**(B1), 741–770.
- Beavan, R.J. & Litchfield, N.J., 2012. *Vertical Land Movement Around the New Zealand Coastline: Implications for Sea-Level Rise*, GNS Science.
- Bertrand, E.A. *et al.*, 2012. Magnetotelluric imaging of upper-crustal convection plumes beneath the Taupo Volcanic Zone, New Zealand, *Geophys. Res. Lett.* **39**(2), L02304, doi:10.1029/2011GL050177.
- Bibby, H.M., Caldwell, T.G., Davey, F.J. & Webb, T.H., 1995. Geophysical evidence on the structure of the Taupo Volcanic Zone and its hydrothermal circulation, *J. Volc. Geotherm. Res.*, **68**(1–3), 29–58.
- Blick, G.H. & Otway, P.M., 1995. *Regional Vertical Deformation from Repeated Precise Levelling in the Taupo Volcanic Zone*, Institute of Geological and Nuclear Sciences Limited.
- Bromley, C.J., Currie, S., Manville, V.R. & Rosenberg, M.D., 2009. Recent ground subsidence at Crown Road, Tauhara and its probable causes, *Geothermics*, **38**(1), 181–191.
- Bryan, C.J., Sherburn, S., Bibby, H.M., Bannister, S.C. & Hurst, A.W., 1999. Shallow seismicity of the central Taupo Volcanic Zone, New Zealand: its distribution and nature, *N. Z. J. Geol. Geophys.*, **42**(4), 533–542.
- Cabral-Cano, E., Correa-Mora, F. & Meertens, C., 2008. Deformation of Popocatepetl volcano using GPS: regional geodynamic context and constraints on its magma chamber, *J. Volc. Geotherm. Res.*, **170**(1–2), 24–34.
- Cardozo, N. & Allmendinger, R.W., 2009. SSPX: A program to compute strain from displacement/velocity data, *Comput. Geosci.*, **35**(6), 1343–1357.
- Cole, J.W., 1990. Structural control and origin of volcanism in the Taupo Volcanic Zone, New Zealand, *Bull. Volcanol.*, **52**(6), 445–459.
- Cole, J.W. & Spinks, K.D., 2009. Caldera volcanism and rift structure in the Taupo Volcanic Zone, New Zealand, in *Ancient Orogens and Modern Analogues*, pp. 9–29, eds Murphy, J.B., Keppie, J.D. & Hynes, A.J., Geological Society Special Publication.
- Cole, J.W., Milner, D.M. & Spinks, K.D., 2005. Calderas and caldera structures: a review, *Earth-Sci. Rev.*, **69**(1–2), 1–26.
- Cole, J.W., Spinks, K.D., Deering, C.D., Baird, I.A. & Leonard, G.S., 2010. Volcanic and structural evolution of the Okataina Volcanic Centre; dominantly silicic volcanism associated with the Taupo Rift, New Zealand, *J. Volc. Geotherm. Res.*, **190**(1–2), 123–135.
- Dach, R., Hugentobler, U., Frizez, P. & Meindl, M., 2007. *Bernese GPS Software Version 5.0*. Stampfli Publications AG, Astronomical Institute, University of Bern.
- Darby, D.J. & Williams, R.O., 1991. A new geodetic estimate of deformation in the Central Volcanic Region of the North Island, New Zealand, *N. Z. J. Geol. Geophys.*, **34**, 127–136.
- Darby, D.J. & Meertens, C.M., 1995. Terrestrial and GPS measurements of deformation across the Taupo back arc and Hikurangi forearc regions in New Zealand, *J. geophys. Res.*, **100**(B5), 8221–8232.
- Darby, D.J., Hodgkinson, K.H. & Blick, G.H., 2000. Geodetic measurement of deformation in the Taupo Volcanic Zone, New Zealand: the North Taupo Network revisited, *N. Z. J. Geol. Geophys.*, **43**(2), 157–170.
- Dixon, T.H., Miller, M., Farina, F., Wang, H.Z. & Johnson, D., 2000. Present-day motion of the Sierra Nevada block and some tectonic implications for the Basin and Range province, North American Cordillera, *Tectonics*, **19**(1), 1–24.
- Ellis, S.M., Wilson, C.J.N., Bannister, S., Bibby, H.M., Heise, W., Wallace, L. & Patterson, N., 2007. A future magma inflation event under the rhyolitic Taupo volcano, New Zealand: Numerical models based on constraints from geochemical, geological, and geophysical data, *J. Volc. Geotherm. Res.*, **168**(1–4), 1–27.

- Ellis, S., Heise, W., Kissling, W., Villamor, P. & Schreurs, G., 2014. The effect of crustal melt on rift dynamics: case study of the Taupo Volcanic Zone, *N. Z. J. Geol. Geophys.*, **57**(4), 453–458.
- Geirsson, H., 2003. *Continuous GPS Measurements in Iceland 1999–2002*. Icelandic Meteorological Office, Reykjavík, Rep. 3014, 94 pp.
- Grindley, G., 1960. *Sheet 8 - Taupo*, D.O.S.a.I. Research, Wellington, New Zealand.
- Hamling, I.J., Hreinsdóttir, S. & Fournier, N., 2015. The ups and downs of the TVZ: geodetic observations of deformation around the Taupo Volcanic Zone, New Zealand, *J. geophys. Res.-Solid Earth*, doi:10.1002/2015JB012125.
- Hole, J.K., Stevens, N.F. & Wadge, G., 2005. Surface deformation at Rotorua, New Zealand measured by InSAR, 1996–2003 (345), in *Envisat and ERS Symposium*, Salzburg, Austria.
- Hole, J.K., Bromley, C.J., Stevens, N.F. & Wadge, G., 2007. Subsidence in the geothermal fields of the Taupo Volcanic Zone, New Zealand from 1996 to 2005 measured by InSAR, *J. Volc. Geotherm. Res.*, **166**(3–4), 125–146.
- Houghton, B.F., Wilson, C.J.N., McWilliams, M.O., Lanphere, M.A., Weaver, S.D., Briggs, R.M. & Pringle, M.S., 1995. Chronology and dynamics of a large silicic magmatic system—Central Taupo Volcanic Zone, New Zealand, *Geology*, **23**(1), 13–16.
- Hugentobler, U. et al., 2001. *Bernese GPS Software, Version 4.2*, Astronomical Institute, University of Berne, Berne, Switzerland.
- International GNSS Service, 2012. *Data Reprocessing Campaign*, IGS Analysis Center Coordinator.
- Kashani, I., Wielgosz, P. & Grejner-Brzezinska, D.A., 2004. On the reliability of the VCV matrix: a case study based on GAMIT and Bernese GPS software, *Gps. Solut.*, **8**(4), 193–199.
- Keir, D., Bastow, I.D., Pagli, C. & Chambers, E.L., 2013. The development of extension and magmatism in the Red Sea rift of Afar, *Tectonophysics*, **607**(0), 98–114.
- Kogan, L., Fisseha, S., Bendick, R., Reilinger, R., McClusky, S., King, R. & Solomon, T., 2012. Lithospheric strength and strain localization in continental extension from observations of the East African Rift, *J. geophys. Res.-Solid Earth*, **117**, B03402, doi:10.1029/2011JB008516.
- Lowry, A.R., Hamburger, M.W., Meertens, C.M. & Ramos, E.G., 2001. GPS monitoring of crustal deformation at Taal Volcano, Philippines, *J. Volc. Geotherm. Res.*, **105**(1–2), 35–47.
- Manville, V. & Wilson, C.J.N., 2003. Interactions between volcanism, rifting and subsidence: implications of intracaldera palaeoshorelines at Taupo volcano, New Zealand, *J. geol. Soc. Lond.*, **160**, 3–6.
- Mao, A.L., Harrison, C.G.A. & Dixon, T.H., 1999. Noise in GPS coordinate time series, *J. geophys. Res.-Solid Earth*, **104**(B2), 2797–2816.
- Means, W.D., 1976. *Stress and Strain*, Springer-Verlag, <http://doi.org/10.1007/978-1-4613-9371-9>.
- Mouslopoulou, V. & Hristopulos, D., 2011. Patterns of tectonic fault interactions captured through geostatistical analysis of microearthquakes, *J. geophys. Res.*, **116**, B07305, doi:10.1029/2010JB007804.
- Mouslopoulou, V., Nicol, A., Little, T.A. & Walsh, J.J., 2007. Terminations of large strike-slip faults: an alternative model from New Zealand, in *Tectonics of Strike-Slip Restraining and Releasing Bends*, pp. 387–415, eds Cunningham, W.D. & Mann, P., Geological Society Special Publication.
- Nairn, I.A., 2002. Geology of the Okataina Volcanic Centre, scale 1:50 000, Institute of Geological and Nuclear Sciences Ltd.
- Nairn, I.A. & Cole, J.W., 1981. Basalt dikes in the 1886 Tarawera Rift, *N. Z. J. Geol. Geophys.*, **24**(5–6), 585–592.
- Neil, A.E., 1996. Global mapping for the atmospheric delay at radio wavelengths, *J. geophys. Res.*, **111**(B2), 3227–3246.
- Payne, S.J., McCaffrey, R., King, R.W. & Kattenhorn, S.A., 2012. A new interpretation of deformation rates in the Snake River Plain and adjacent basin and range regions based on GPS, *Geophys. J. Int.*, **118**(1), 101–122.
- Price, R.C., Gamble, J.A., Smith, I.E.M., Stewart, R.B., Egging, S. & Wright, I.C., 2005. An integrated model for the temporal evolution of andesites and rhyolites and crustal development in New Zealand's North Island, *J. Volc. Geotherm. Res.*, **140**(1–3), 1–24.
- Pulford, A. & Stern, T., 2004. Pliocene exhumation and landscape evolution of central North Island, New Zealand: the role of the upper mantle, *J. geophys. Res.-Solid Earth*, **109**, F01016, doi:10.1029/2003JF000046.
- Puskas, C.M., Smith, R.B., Meertens, C.M. & Chang, W.L., 2007. Crustal deformation of the Yellowstone-Snake River Plain volcano-tectonic system: campaign and continuous GPS observations, 1987–2004, *J. geophys. Res.-Solid Earth*, **112**(B3), B03401, doi:10.1029/2006JB004325.
- Rowland, J.V. & Sibson, R.H., 2001. Extensional fault kinematics within the Taupo Volcanic Zone, New Zealand: soft-linked segmentation of a continental rift system, *N. Z. J. Geol. Geophys.*, **44**(2), 271–283.
- Rowland, J.V., Wilson, C.J.N. & Gravley, D.M., 2010. Spatial and temporal variations in magma-assisted rifting, Taupo Volcanic Zone, New Zealand, *J. Volc. Geotherm. Res.*, **190**(1–2), 89–108.
- Sagiya, T., Miyazaki, S. & Tada, T., 2000. Continuous GPS array and present-day crustal deformation of Japan, *Pure appl. Geophys.*, **157**(11–12), 2303–2322.
- Samsonov, S., Beavan, J., Gonzalez, P.J., Tiampo, K. & Fernandez, J., 2011. Ground deformation in the Taupo Volcanic Zone, New Zealand, observed by ALOS PALSAR interferometry, *Geophys. J. Int.*, **187**(1), 147–160.
- Scott, B.J., 1989. Geodetic and geophysical monitoring of the 1886 Tarawera rift, in *Volcanic Hazards Assessment and Monitoring, IAVCEI Proceedings in Volcanology*, pp. 575–584, ed. Latter, J.H., Springer-Verlag.
- Scott, B.J., 1992. *Characteristics of Cyclic activity in Frying Pan and Inferno Crater Lakes, Waimangu, New Zealand Geothermal Workshop*, Institute of Geological and Nuclear Sciences contribution Auckland, 253–258 pp.
- Scott, B.J., 1994. Cyclic activity in the Crater Lakes of Waimangu hydrothermal system, New Zealand. *Geothermics*, **23**(5–6), 555–572.
- Seebeck, H. & Nicol, A., 2009. Dike intrusion and displacement accumulation at the intersection of the Okataina Volcanic Centre and Paeroa Fault zone, Taupo Rift, New Zealand, *Tectonophysics*, **475**(3–4), 575–585.
- Seebeck, H., Nicol, A., Stern, T.A., Bibby, H.M. & Stagpoole, V., 2010. Fault controls on the geometry and location of the Okataina Caldera, Taupo Volcanic Zone, New Zealand, *J. Volc. Geotherm. Res.*, **190**(1–2), 136–151.
- Serpelloni, E., Anzidei, M., Baldi, P., Casula, G. & Galvani, A., 2006. GPS measurement of active strains across the Apennines, *Ann. Geophys.-Italy*, **49**(1), 319–329.
- Sherburn, S. & Nairn, I.A., 2004. Modelling geophysical precursors to the prehistoric c. AD1305 Kaharoa rhyolite eruption of Tarawera volcano, New Zealand, *Nat. Hazards*, **32**(1), 37–58.
- Smith, V.C., Shane, P. & Nairn, I.A., 2005. Trends in rhyolite geochemistry, mineralogy, and magma storage during the last 50 kyr at Okataina and Taupo volcanic centres, Taupo Volcanic Zone, New Zealand, *J. Volc. Geotherm. Res.*, **148**(3–4), 372–406.
- Smith, V.C., Shane, P. & Nairn, I.A., 2010. Insights into silicic melt generation using plagioclase, quartz and melt inclusions from the caldera-forming Rotoiti eruption, Taupo volcanic zone, New Zealand, *Contrib. Miner. Petr.*, **160**(6), 951–971.
- Spinks, K.D., Acocella, V., Cole, J.W. & Bassett, K.N., 2005. Structural control of volcanism and caldera development in the transtensional Taupo Volcanic Zone, New Zealand, *J. Volc. Geotherm. Res.*, **144**(1–4), 7–22.
- Sutton, A.N., Blake, S., Wilson, C.J.N. & Charlier, B.L.A., 2000. Late Quaternary evolution of a hyperactive rhyolite magmatic system: Taupo volcanic centre, New Zealand, *J. geol. Soc. Lond.*, **157**, 537–552.
- Tenzer, R., Stevenson, M. & Denys, P., 2012. A compilation of a preliminary map of vertical deformations in New Zealand from continuous GPS data, *Iag Symp.*, **136**, 697–703.
- Tregoning, P., Burgette, R., McClusky, S.C., Lejeune, S., McQueen, H. & Watson, C.S., 2013. A decade of horizontal deformation from great earthquakes, *J. geophys. Res.-Solid Earth*, **118**, doi:10.1002/jgrb.50154.
- Vandemeulebrouck, J., Hurst, A.W. & Scott, B.J., 2008. The effects of hydrothermal eruptions and a tectonic earthquake on a cycling crater lake (Inferno Crater Lake, Waimangu, New Zealand), *J. Volc. Geotherm. Res.*, **178**(2), 271–275.
- Vigny, C., de Chabalier, J.B., Ruegg, J.C., Huchon, P., Feigl, K.L., Catlin, R., Asfaw, L. & Kanbari, K., 2007. Twenty-five years of geodetic measurements along the Tadjoura-Asal rift system, Djibouti, East Africa, *J. geophys. Res.-Solid Earth*, **112**, B06410, doi:10.1029/2004JB003230.

- Villamor, P. & Berryman, K., 2001. A late Quaternary extension rate in the Taupo Volcanic Zone, New Zealand, derived from fault slip data, *N. Z. J. Geol. Geophys.*, **44**(2), 243–269.
- Villamor, P. & Berryman, K.R., 2006. Evolution of the southern termination of the Taupo Rift, New Zealand, *N. Z. J. Geol. Geophys.*, **49**(1), 23–37.
- Villamor, P., Berryman, K.R., Nairn, I., Van Dissen, R., Begg, J. & Lee, J., 2008. Late Pleistocene surface rupture history of the Paeroa Fault, Taupo Rift, New Zealand, *N. Z. J. Geol. Geophys.*, **51**(1), 135–158.
- Walcott, R.I., 1987. Geodetic strain and the deformational history of the North Island of New Zealand during the Late Cainozoic, *Phil. Trans. R. Soc. Lond. A.*, **321**(1557), 163–181.
- Wallace, L.M., Beavan, J., McCaffrey, R. & Darby, D., 2004. Subduction zone coupling and tectonic block rotations in the North Island, New Zealand, *J. geophys. Res.-Solid Earth*, **109**(B12), B12406, doi:10.1029/2004JB003241.
- Wessel, P. & Smith, W.H.F., 1998. New version of the generic mapping tools released, *EOS, Trans. Am. geophys. Un.*, **79**(47), 579.
- Williams, S.D.P., Bock, Y., Fang, P., Jamason, P., Nikolaidis, R.M., Prawirodirdjo, L., Miller, M. & Johnson, D.J., 2004. Error analysis of continuous GPS position time series, *J. geophys. Res.-Solid Earth*, **109**(B3), B03412, doi:10.1029/2003JB002741.
- Wilson, C.J.N. & Charlier, B.L.A., 2009. Rapid rates of magma generation at contemporaneous magma systems, Taupo Volcano, New Zealand: insights from U-Th model-age spectra in Zircons, *J. Petrol.*, **50**(5), 875–907.
- Wilson, C.J.N., Houghton, B.F., McWilliams, M.O., Lanphere, M.A., Weaver, S.D. & Briggs, R.M., 1995. Volcanic and structural evolution of Taupo Volcanic Zone, New Zealand: a review, *J. Volc. Geotherm. Res.*, **68**(1–3), 1–28.
- Wright, I.C., 1990. Late Quaternary faulting of the offshore Whakatane Graben, Taupo Volcanic Zone, New Zealand, *N. Z. J. Geol. Geophys.*, **33**(2), 245–256.
- Zhang, J., Bock, Y., Johnson, H., Fang, P., Williams, S., Genrich, J., Wdowinski, S. & Behr, J., 1997. Southern California permanent GPS geodetic array: error analysis of daily position estimates and site velocities, *J. geophys. Res.-Solid Earth*, **102**(B8), 18 035–18 055.